Loss of SUMO-specific protease 2 causes isolated glucocorticoid deficiency by blocking adrenal cortex zonal transdifferentiation

Damien Dufour [1], Typhanie Dumontet [1,2,3], Isabelle Sahut-Barnola [1], Meline Onzon [1], Eric Pussard [4], James Jr Wilmouth [1], Julie Olabe [1], Cecily Lucas [1,5], Adrien Levasseur [1], Christelle Soubeyrand-Damon [1], Jean-Christophe Pointud [1], Florence Roucher-Boulez [1,5], Igor Tauveron [1,6], Guillaume Bossis [7], Edward T.Yeh [8], David T. Breault [9,10], Pierre Val [1], Anne-Marie Lefrançois-Martinez [1] and Antoine Martinez [1*]

[1] institut Génétique, Reproduction & Développement (iGReD), CNRS, INSERM, Université Clermont Auvergne, Clermont–Ferrand, F-63000, France. [2] Department of Internal Medicine, Division of Metabolism, Endocrinology, and Diabetes, University of Michigan, Ann Arbor, Michigan, USA. [3] Training Program in Organogenesis, Center for Cell Plasticity and Organ Design, University of Michigan, Ann Arbor, Michigan, USA. [4] Service de Génétique Moléculaire, Pharmacogénétique et Hormonologie, Hôpital de Bicêtre, Assistance Publique-Hôpitaux de Paris (APHP), Physiologie et Physiopathologie Endocriniennes, INSERM, Université Paris-Saclay, Le Kremlin-Bicêtre, France. [5] Endocrinologie Moléculaire et Maladies Rares, Centre Hospitalier Universitaire, Université Claude Bernard Lyon 1, Bron, France. [6] Service d'Endocrinologie, Centre Hospitalier Universitaire Gabriel Montpied, Université Clermont Auvergne, Clermont-Ferrand, France. [7] IGMM, Université de Montpellier, CNRS, Montpellier, France. [8] Department of Internal Medicine, University of Arkansas for Medical Sciences, Little Rock, Arkansas, USA. [9] Division of Endocrinology, Boston Children's Hospital, Department of Pediatrics, Harvard Medical School, Boston, Massachusetts, USA. [10] Harvard Stem Cell Institute, Harvard University, Cambridge, Massachusetts, USA.

*Corresponding author(s). E-mail(s): antoine.martinez@uca.fr; Contributing authors: damien.dufour@doctorant.uca.fr; tdumonte@med.umich.edu; isabelle.barnola@uca.fr; meline.onzon@etu.uca.fr ; eric.pussard@aphp.fr; jwilmouth21@gmail.com; julie.olabe@gmail.com; cecily.lucas6@gmail.com; Adrien.levasseur@uca.fr; christelle.soubeyrand-damon@uca.fr j-christophe.pointud@uca.fr; florence.roucher@chu-lyon.fr; itauveron@chu-clermontferrand.fr; guillaume.bossis@igmm.cnrs.fr; dredyeh@gmail.com; david.breault@childrens.harvard.edu; pierre.val@uca.fr; a-marie.lefrancois-martinez@uca.fr;

Abstract

SUMOylation is a dynamic posttranslational modification, that provides fine-tuning of protein function involved in the cellular response to stress, differentiation, and tissue development. In the adrenal cortex, an emblematic endocrine organ that mediates adaptation to physiological demands, the SUMOylation gradient is inversely correlated with the gradient of cellular differentiation raising important questions about its role in functional zonation and the response to stress. Considering that SUMO-specific protease 2 (SENP2), a deSUMOylating enzyme, is upregulated by ACTH/PKA signalling within the zona *Fasciculata* (zF), we generated mice with adrenal-specific *Senp2* loss to address these questions. Disruption of SENP2 activity in steroidogenic cells leads to specific hypoplasia of the zF, a blunted reponses to ACTH and isolated glucocorticoid deficiency. Mechanistically, overSUMOylation resulting from SENP2 loss shifts the balance between ACTH/PKA and WNT/β-catenin signalling leading to repression of PKA activity and ectopic activation of β-catenin. At the cellular level, this blocks transdifferentiation of β-catenin-positive zona *Glomerulosa* cells into zF cells and sensitises them to premature apoptosis. Our findings indicate that the SUMO pathway is critical for adrenal homeostasis and stress responsiveness.

Keywords: Adrenal, SUMO, SENP2, β-catenin, PKA, DRP1

The adrenal cortex is a constantly self-renewed endocrine organ composed of concentric zones, including the outermost *zona glomerulosa* (zG) layer producing mineralocorticoids and the innermost *zona fasciculata* (zF) layer producing glucocorticoids. According to the centripetal migration model occurring during postnatal development, progenitors cell populations located in the adrenal capsule (characterised by GLI1 expression) or within the zG (characterised by SHH expression) consecutively differentiate into steroid-producing zG cells, then through a process of zonal transdifferentiation, convert into zF cells before eventually undergoing apoptosis at the corticomedullary junction[1–3].

Genetic models and *in vitro* approaches have identified two important signalling pathways for adrenal cortex homeostasis. On the one hand, the WNT/Rspondin/β-catenin pathway is necessary for the maintenance of progenitor pools and the acquisition of zG identity[4–6]. On the other hand, cAMP/PKA signalling, stimulated by pituitary ACTH, triggers the recruitment of progenitors by inducing the transdifferentiation of zG cells into zF cells and stimulates glucocorticoids production[7,8]. We and others have previously shown that these two signalling pathways antagonise each other by modulating various actors such as WNT4, PDE2A or CCDC80[3,6,9]. Optimal response to PKA signalling and therefore zF differentiation is also subject to epigenetic programming by the histone methyl transferase EZH2[10]. Nonetheless, the mechanisms that maintain adrenal cortex zonation and balance between these two pathways are yet to be discovered.

SUMOylation is a dynamic and one of the fastest evolving[11] posttranslational modification consisting in the covalent addition of SUMO peptides on a target protein. This modification can affect various processes such as protein stability, interactions or subcellular localisation[12]. There are three main SUMO peptides in rodents, namely SUMO1, which shares around 50% of identity with SUMO2 and SUMO3, the two latter differing by only three amino acids. SUMOylation is achieved through an enzymatic cascade involving activation by the E1 heterodimer (SAE1/UBA2), conjugation by the sole E2 enzyme UBC9 (encoded by *Ube2i*) and final ligation by various E3 SUMO ligases such as members of the PIAS and TRIM families as well as RANBP2 and CBX4.[13,14] SUMO peptides can be removed from SUMO-conjugated substrates by deSUMOylases belonging mainly to the Sentrin-specific proteases family (SENPs) or by the more recently discovered DeSI-1 and USPL1 making this posttranslational modification highly dynamic (Figure S1.A.B.). Several *in vitro* and *in vivo* studies have highlighted the importance of controlling SUMOylation levels to enable differentiation or maintain cellular identity[15–17] and tissue homeostasis *in vivo* in various cell lineages[18,19]. The adrenal gland could provide a paradigm to study how SUMOylation dynamics can interact with the function and homeostasis of an organ, in charge of constant adaptation to stress.

We have previously shown that protein SUMOylation follows a decreasing centripetal gradient in human and mouse normal adrenal cortices. Moreover, this gradient is altered in genetic endocrine diseases with deregulated PKA or WNT signalling pathways[20]. Remarkably, SUMOylation is negatively and acutely regulated by ACTH in both adrenal cortex and adrenocortical cell cultures through transcriptional control of key enzymes, especially SENP2 whose upregulation by PKA correlates with transient hypoSUMOylation in zF. Interestingly, PKA-mediated up-regulation of *Senp2* was previously shown to promote the progression of

preadipocytes into the adipogenic program[15]. Taken together, these studies suggest that limiting SUMOylation may facilitate or be a prerequisite for any change in differentiation states. Conversely, an excess of WNT/β-catenin signalling in the adrenal cortex induces an expansion of zG identity that is correlated with a high SUMOylation state[20]. Finally, preventing *in vivo* SUMOylation of the transcription factor SF-1 (*SF-1*$^{2KR/2KR}$ mice), the main driver of adrenogonadal cell fate, disturbs endocrine development by maintaining discrete gonadal traits in the cortex and adrenal traits in the testis[21]. This highlights the need to control SUMOylation during cell fate decisions leading to adrenal cortex identity.

We hypothesise that disruption of the SUMOylation gradient in the adrenal cortex may disrupt zonation and impair adaptive response to stress. In order to understand the implication of SUMO pathway on homeostatic maintenance and endocrine function, we have developed mouse models of adrenal hyperSUMOylation by conditional ablation of *Senp2* in the cortex (*Senp2*^{cKO}). Our report reveals that *Senp2*^{cKO} mice show zone-specific adrenal atrophy, isolated glucocorticoid deficiency and blunted response to ACTH. Progressive atrophy of zF evoked by SENP2 deficiency results from a blockade of zonal transdifferentiation, early apoptosis and impaired PKA catalytic activity that cannot be rescued by genetic derepression of the PKA holoenzyme. SENP2-deficient adrenals also show increased β-catenin SUMOylation and activity that may help to antagonise PKA signalling, thus maintaining the suppression of zF identity. As *Senp2* expression is itself under the control of ACTH/PKA, our data identify SUMOylation as a feedforward mechanism that readies the adrenal cortex to respond to stress and maintain functional zonation.

Results

Senp2 invalidation in the adrenal cortex leads to zF hypoplasia and adrenal dysplasia

To assess the role of SUMOylation in the adrenal cortex, we have developed a mouse model with specific deletion of the ACTH-regulated deSUMOylase SENP2[20] in steroidogenic cells by mating *Senp2*$^{fl/fl}$ mice[22] with *SF-1(Nr5a1)*-Cre mice[23]. *Senp2* conditional knock-out mice are later referred to as *Senp2*^{cKO}. *Senp2* deletion was confirmed in 4-week-old mouse adrenals by RT-qPCR analyses showing reduced *Senp2* mRNA accumulation in both genders and by genomic PCR, confirming adrenal-specific recombination at the *Senp2 locus* (Figure S1.C.D.).

Monitoring of adrenal mass from 4 to 40 weeks of age revealed significant adrenal hypoplasia in mutants, occurring between 4 and 8 weeks in both sexes. After this time point, overall adrenal weight in *Senp2*^{cKO} remained below that of controls in females only because of sex differences in the kinetics of adrenal mass gain (almost continuous growth in WT females contrasting with a progressive decrease in WT males over time) (Figure 1.A.). To investigate the causes of this hypoplasia, we performed H&E staining, which revealed two different histological phenotypes: either homogeneous atrophy of the cortex leaving medulla centrally located, or cortical atrophy accompanied by dysplasia due to clusters of large eosinophilic

cells, usually at one pole of the gland and pushing the medulla toward the other pole (Figure 1.B. left panel).

Immunofluorescence co-staining for zonal markers showed that, compared to WT, the integrity of zG (DAB2+) did not seem affected in *Senp2*^{cKO} adrenals of 8-week-old mice, while zF (AKR1B7+) was atrophic and sometimes mislocated together with the medulla (TH+) in dysplastic glands (Figure 1.B. right panels). To confirm that the zF was the most affected by *Senp2* invalidation, the number of cells in each cortical zones and medulla was counted on 2D sections. This showed a dramatic and specific reduction in total cortical cell number regardless of sex, solely attributable to the 75-80% loss of zF cells (Figures 1.C. & S1.E). Laminin immunostaining was then used to examine vascular architecture in WT and mutant adrenal sections. Typical capillaries surrounding the "rosette" structures in the zG and delimiting the zF cells columns were evidenced in WT adrenal sections. Consistent with zonal markers immunostaining, a rosette-like pattern of vascularisation, typical of zG, was found in areas with atrophic zF (Figure 1.B.a.), whereas large columnar structures surrounding clusters of hypertrophic zF cells were evidenced in dysplastic *Senp2*-deficient glands (Figure 1.B.b.).

To further characterise the origin of adrenal dysplasia, we introduced the *Rosa26RmTmG* reporter transgene[24] (Figure S1.F.) into *Senp2*^{cKO} background to trace *Senp2* recombination using GFP immunostaining and non-recombined cells using Tomato immunostaining. WT adrenals (from *Sf1-Cre/+::Senp2*$^{fl/+}$*::R26R*$^{mTmG/mTmG}$ triple transgenic mice) presented full recombined cortex, while in dysplastic *Senp2*^{cKO} adrenals (*Sf1-Cre/+::Senp2*$^{fl/fl}$*::R26R*$^{mTmG/mTmG}$), most of the cells belonging to the mislocated zF were GFP-negative/Tomato-positive, hence non recombined (Figure 1.D.). To address the identity of these cells escaping recombination, we performed co-staining of GFP with the canonical steroidogenic marker SF-1. Surprisingly, GFP-negative cells expressed SF-1, implying that they kept full steroidogenic identity (Figure 1.D. bottom centre panel) as also suggested by detection of zonal markers (Figure 1.B. right panels, bottom). To confirm that these cells were hypertrophic as H&E and Laminin staining suggested, we measured 2D cell areas in the zF of WT and *Senp2*^{cKO} adrenal sections. This showed that in females, although GFP-positive and GFP-negative zF cell areas did not differ in the mutant, GFP-negative cells were larger than zF cells from WT adrenals (Figure 1.E.). Similar observations were made in males but with a *P*-value of 0.0560. Next, we assessed global SUMOylation status by western blot and found no variation in the profile of SUMO1 or SUMO2/3 conjugates as a function of the genotype (Figure S1.G.H.). However, GFP-positive zF cells retained nuclear SUMO2/3 staining whereas GFP-negative had diffuse staining in the cytoplasm (Figure S1.I.J.). Together, these results indicate that the clusters of cellular hypertrophy found in dysplastic *Senp2*^{cKO} adrenals are predominantly composed of zF cells that have escaped *Senp2* ablation and that this phenotype (hypertrophic zF clusters) seems more likely to occur in females. To examine further this sexual dimorphism, we assessed the proportion of mutant adrenals presenting with hypertrophic zF clusters from 4 to 40 weeks of age in both genders (Figure 1.F.). Throughout time, the frequency of adrenals with hypertrophic zF clusters increased in a sexually dimorphic fashion: indeed, for these clusters to develop in all adrenals, it took 40 weeks in males and only 24 in females. Thus, in 40-week-old mice, *Senp2*^{cKO} adrenal cortex contained, compared to WT, very few GFP-positive zF cells, with

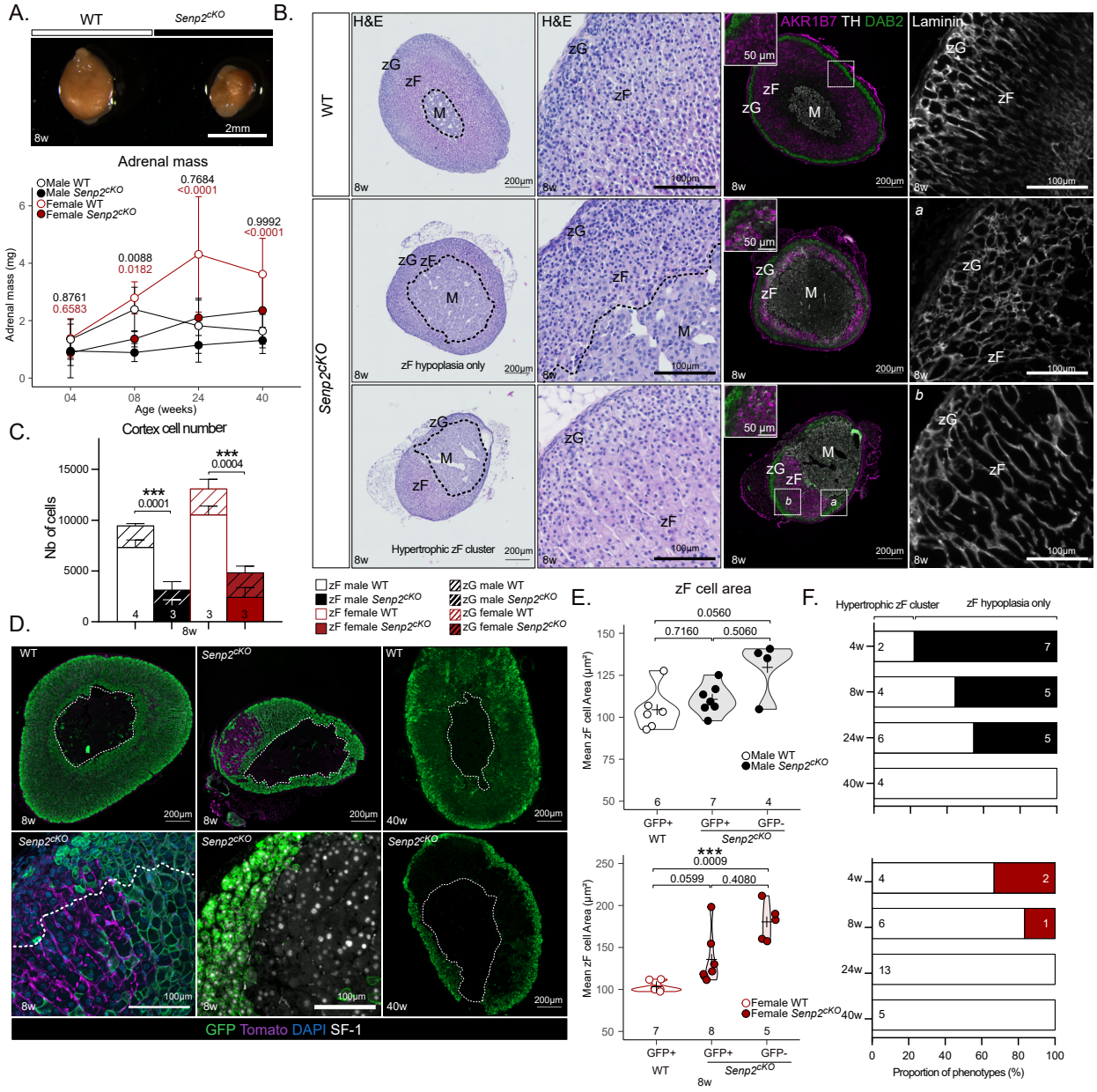

Figure 1: **Deletion of the deSUMOylase *Senp2* in embryonic steroidogenic cells induces adrenal dysplasia and zF hypoplasia in adult mice.**

A. Top : Representative picture of an 8-week-old WT (left) and a *Senp2*^{cKO} (right) adrenal.
Bottom : Absolute adrenal mass follow-up of male and female mice WT and *Senp2*^{cKO} (mean) from 4 to 40 weeks of age. *P*-values represent difference between genotypes within the same age and sex group.

B. Morphological analysis of the phenotypes on 8-week-old males' adrenals. Left : H&E staining of WT or *Senp2*^{cKO} adrenals with or without dysplasia. Center : Coimmunofluorescence labelling of AKR1B7 (green), TH/Tyrosine Hydroxylase (white) and DAB2/Disabled2 (Purple) in WT and *Senp2*^{cKO} adrenals. Right : Immunofluorescence analysis of laminin (white) revealing the vascular network in WT and cKO adrenals.

C. 2D cell number counting in male and female adrenals at 8 weeks of age.

D. Coimmunofluorescence labelling of GFP (green) with Tomato (purple) and SF-1 (white) at 8 (left and center) and 40 weeks of age (right) WT and *Senp2*^{cKO} adrenals.

E. Morphometric analysis of zF cells area in WT (GFP+) adrenals and recombined (GFP+) or non recombined (GFP-) zones of *Senp2*^{cKO} adrenals at 8 weeks of age.

F. Prevalence of phenotypes in cKO adrenals at different ages. Black (male) or red (female) bars represent hypoplastic adrenals without any gross morphological change and white bar represents hypoplastic and dysplastic adrenals harbouring hypertrophic zF clusters.

zG, *zona glomerulosa*; zF, *zona fasciculata*; WT, wild-type; cKO, conditional Knock-Out.

GFP staining limited to zG and non-recombined cells constituting the entire zF (Figures 1.D. right panel & S1.K.).

Altogether, these results show that SENP2 is necessary for proper adrenal cortex zonation and homeostatic maintenance. Indeed, its inactivation initially leads, to zF atrophy, which is compensated over time by the recruitment of cells escaping *Senp2* recombination allowing them to maintain a wild-type *Senp2* zF in otherwise mutant adrenals. Importantly, we show that females more efficiently overcome zF atrophy induced by *Senp2* loss. This further highlights the sexually dimorphic traits of adrenal homeostasis[25,26].

Loss of SENP2 is associated with isolated glucocorticoid deficiency

Given the profound alterations and notably, the time and sex-dependant remodelling of adrenal cortex zonation in $Senp2^{cKO}$, we measured changes in circulating steroid levels and assessed steroidogenic gene expression. Steroid hormones are synthesised from cholesterol through enzymatic processes resulting in corticosterone production by zF cells and aldosterone by zG cells (Figure 2.A.). Since zF was the most impacted zone by the *Senp2* mutation, we anticipated a reduction in plasmatic corticosterone levels, the main glucocorticoid in rodents. Indeed, compared to control males, corticosterone levels were dramatically reduced in $Senp2^{cKO}$ at 4 weeks and remained lower at 8 weeks of age. Interestingly, levels normalised over time to be indistinguishable from controls by 24 weeks (Figure 2.B. top). In contrast, *Senp2* inactivation had no impact on corticosterone concentrations in females, at any time point (Figure 2.B. bottom). The integrity of the zF and the corticosterone production are under the strict control of pituitary ACTH that maintains homeostasis through a negative feedback loop mediated by the glucocorticoids on the hypothalamic-pituitary-adrenals (HPA) axis. Therefore, we measured circulating ACTH in $Senp2^{cKO}$ and found a 8- 10-fold increase at 24 weeks in both sexes. This is consistent with a dysfunction of the zF cells, resulting in a subclinical insufficiency over time (Figure 2.C.).

For insights into the mechanisms of this insufficiency, we analysed the expression of steroidogenic genes in adrenals of 4-week-old mice. RT-qPCR analyses showed that mRNA levels of *Star* and *Cyp11a1* encoding rate limiting step proteins in steroidogenesis, were decreased in both male and female $Senp2^{cKO}$ adrenals (Figure 2.D.). Interestingly, *Cyp21a1*, *Hsd3b1* and *Cyp11b1* transcripts were specifically downregulated in female $Senp2^{cKO}$ adrenals (Figure 2.D). To assess the impact of *Senp2* loss on zG function, we measured mineralocorticoids plasma levels and *Cyp11b2* expression. Consistently with histological observations, we did not find any negative effect of *Senp2* ablation on aldosterone levels, but rather a positive trend with an increase in 18-hydroxy-corticosterone plasmatic concentration in $Senp2^{cKO}$ males at 24 weeks and a trend toward upregulation of *Cyp11b2* expression in $Senp2^{cKO}$ female adrenals at 4 weeks (Figure S2.A.B.C.).

In conclusion, these results draw a picture of the differential role of *Senp2* in the zonation of the adrenal cortex. While it is dispensable for the zG, its absence leads to a deficient zF struggling to produce enough corticosterone to maintain homeostasis. This effort is illustrated by elevated circulating ACTH and hypertrophic zF cells, hallmarks of isolated glucocorticoid deficiency.

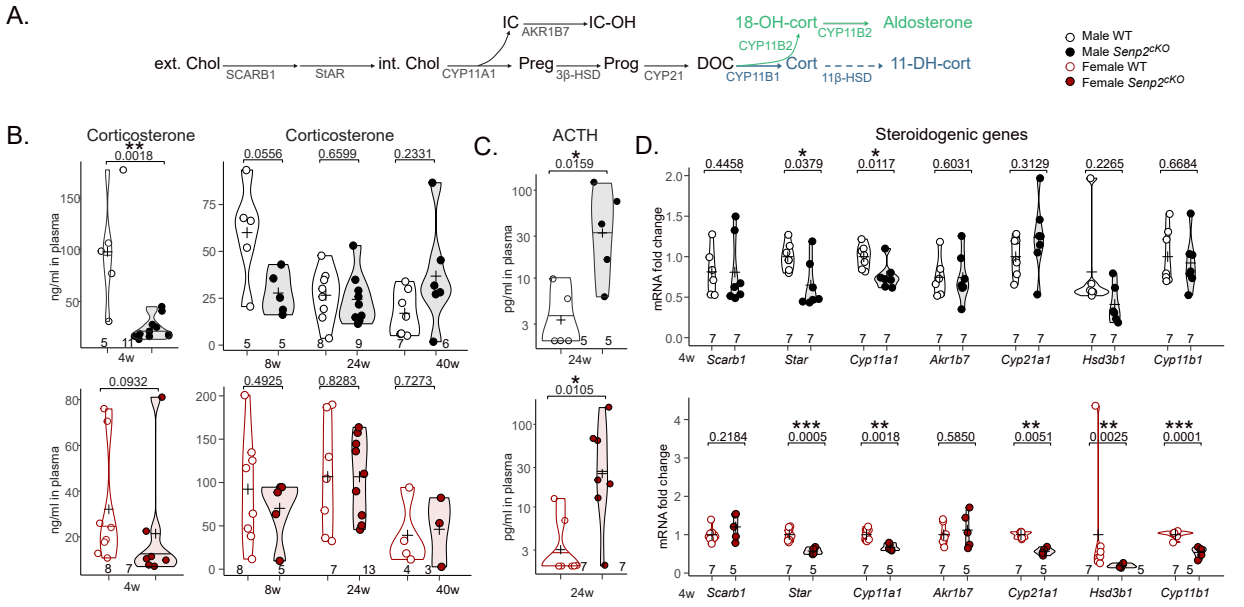

Figure 2: ***Senp2* invalidation induces isolated glucocorticoid insufficiency.**
A. Schematic representation of gluco- (blue) and mineralo- (green) corticoids synthesis : ext.Chol/int.Chol, extra/intracellular cholesterol; Preg, pregnenolone; Prog, progesterone; DOC, 11-deoxy-corticosterone; cort, corticosterone; 18-OH-cort, 18-hydroxycorticosterone; including detoxication of cholesterol side-chain clivage IC (Isocaproaldehyde) into IC-OH (isocapryl alcohol) and inactivation of corticosterone into 11-DH-cort (11-dehydrocorticosterone).
B. Plasmatic concentration of corticosterone in WT and $Senp2^{cKO}$ at 4 (determined by ELISA), 8, 24 and 40 weeks of age (determined by LC-MS/MS).
C. ACTH plasmatic levels of 24-week-old WT and $Senp2^{cKO}$ mice.
D. qPCR analyses of steroidogenic genes mRNA accumulation in 4-week-old WT and $Senp2^{cKO}$ mice.

Adrenal cortex lacking *Senp2* shows blunted ACTH response

To understand the underpinnings of the adrenal phenotype in $Senp2^{cKO}$ mice, knowing that ACTH is a regulator of SUMOylation in the adrenal cortex[20], we assessed the endocrine and transcriptional steroidogenic responses to acute ACTH stimulation. Plasma concentrations of steroids associated with glucocorticoid metabolism (Figure 2.A.) were determined by LC-MS/MS, in 24-week-old mice injected 2 hours before with ACTH and compared to vehicle (Figure 3.A. & Table 1.). We confirmed that, at this age, there were no differences in plasma levels of all steroids measured in basal conditions (vehicle) between WT and $Senp2^{cKO}$ mice. As expected, ACTH treatment induced a strong increase in adrenal steroids (*e.g.* corticosterone levels were 3- to 7-fold induced in females and males, respectively) in plasma from WT mice (except progesterone in females, which comes mainly from the ovaries). However, the ACTH-stimulated endocrine response was heavily blunted and at least halved in $Senp2^{cKO}$ mice (Table 1.). To determine whether alteration of endocrine response correlated with changes in gene expression, we measured mRNA levels of ACTH-responsive genes involved in initial steps of steroidogenesis (*i.e. Scarb1* and *Star*) by RT-qPCR (Figure 3.B.). In males, *Senp2* mutation did not alter *Scarb1* and *Star* transcriptional responsiveness to ACTH (1.5- to 2-fold induction after 2h) but impaired their basal expression, so that mRNA levels in ACTH-treated mutant adrenals barely reached basal expression in controls. By contrast in females, although their basal expression remained unchanged, both *Scarb1* and

Star genes entirely failed to respond to ACTH in *Senp2*^{cKO} adrenals (Figure 3.B.). To test whether this blunted transcriptional response relied on changes in phosphorylation of PKA substrates (Figure S3.A.), we performed western blots on trans-acting factor CREB and SUMO E3 ligase TRIM28, in response to 30 min ACTH treatment, in WT and mutant mice. Ser133 CREB and Ser473 TRIM28 phosphorylation levels were similar in basal conditions, increased in WT upon ACTH stimulation but failed to respond to treatment in *Senp2*^{cKO} adrenals (Figure 3.C.). This impaired response to ACTH/PKA-mediated phosphorylation was unlikely caused by altered expression of ACTH receptor and co-receptor (*Mc2r* and *Mrap*, respectively) that were unaltered by *Senp2* loss (Figure S3.B.).

			ACTH	
	Mean concentration +/- SD (*P* -value compared to vehicle counterpart)			
Male	WT	*Senp2* cKO	WT	*Senp2* cKO
Progesterone	0.15 +/- 0.09	0.30 +/- 0.39	9.23 +/- 4.03 (**0.0001**)	1.70 +/- 0.88 (**0.0457**)
DOC	0.31 +/- 0.29	0.43 +/- 0.17	24.02 +/- 18.9 (**0.0001**)	5.26 +/- 3.53 (**0.0401**)
Corticosterone	26.6 +/- 13.89	24.39 +/- 13.36	202.3 +/- 40.96 (**0.0001**)	75.53 +/- 22.10 (**0.0267**)
11-DH-cort	0.13 +/- 0.11	0.12 +/- 0.06	0.89 +/- 0.68 (**0.0004**)	0.18 +/- 0.06 (0.3815)

			ACTH	
	Mean concentration +/- SD (*P* -value compared to vehicle counterpart)			
Female	WT	*Senp2* cKO	WT	*Senp2* cKO
Progesterone	7.31 +/- 15.52	5.56 +/- 11.57	3.55 +/- 1.62 (0.9999)	2.60 +/- 1.08 (0.2182)
DOC	4.91 +/- 4.20	9.65 +/- 11.53	55.75 +/- 14.29 (**0.0001**)	28.02 +/- 13.62 (0.0896)
Corticosterone	106.70 +/- 65.69	112.80 +/- 47.87	334.20 +/- 67.24 (**0.0001**)	200.00 +/- 81.52 (**0.0113**)
11-DH-cort	0.49 +/- 0.33	0.45 +/- 0.18	2.30 +/- 1.01 (**0.0001**)	0.85 +/- 0.36 (0.1544)

Kruskal-Wallis with multiple comparisons using Dunn's test to determine the genotype or treatment effect

Table 1: **Mean steroids plasmatic concentrations after 2 hours ACTH treatment**

To determine whether the deficiency in ACTH response involved PKA holoenzyme or occurred upstream of the kinase, we assessed the capacity of genetic activation of PKA to rescue adrenal insufficiency in *Senp2*^{cKO} mice by removing the RIα subunit (*Prkar1a* floxed allele) known to repress PKA catalytic activity[7,9,27]. As expected, 4-week-old *Prkar1a*^{cKO} mice developed large adrenals with hyperplastic zF and atrophic zG (Figure S3.C.D.). Adrenals from *Senp2,Prkar1a*^{dcKO} and *Senp2*^{cKO} mice were both dysplastic and showed reduction in cortical cell numbers. However, *dcKO* adrenals showed an atrophic zG (loss of DAB2 staining) presumably resulting from the antagonistic action of PKA signalling on zG identity (Figures 3.D. & S3.C.D.)[7,9]. As a result, in the absence of NaCl supplementation, *Senp2,Prkar1a*^{dcKO} mice died prematurely from salt wasting (Figure S3.E.), whereas *Senp2*^{cKO} mice only suffered from isolated glucocorticoid deficiency. Thus, genetic derepression of PKA was unable to overcome cortical atrophy and dysplasia imparted by *Senp2* deficiency. This suggested

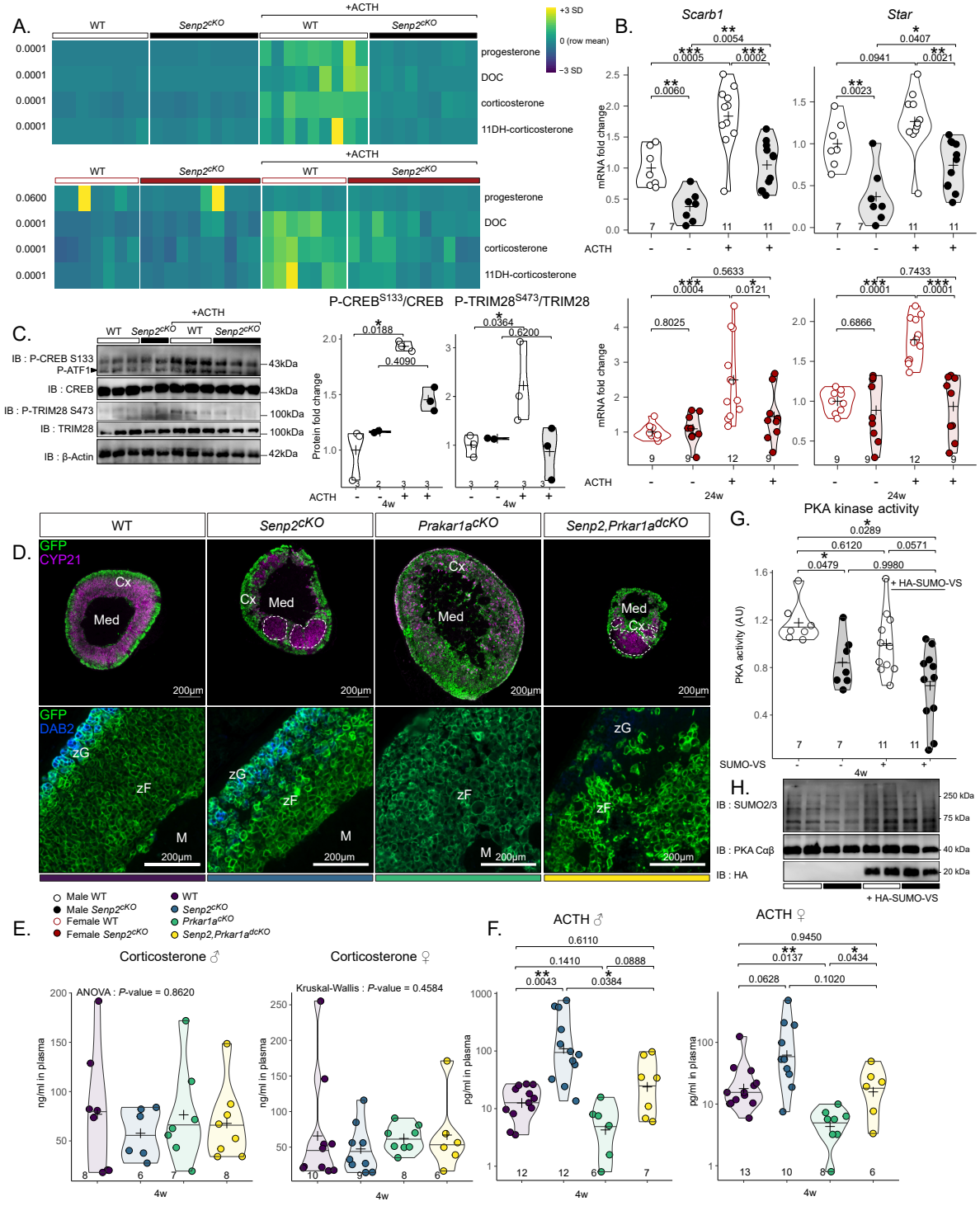

Figure 3: ***Senp2* is necessary for proper ACTH response**.

A. Heatmap representing the plasmatic concentration of progesterone, DOC, corticosterone and 11-dehydrocorticosterone after treatment with PBS or ACTH for 2 h determined by LC-MS/MS in WT or $Senp2^{cKO}$ 24-week-old mice.

B. qPCR analysis of ACTH responsive genes mRNA accumulation in 24-week-old WT and $Senp2^{cKO}$ mice after treatment with PBS or ACTH for 2 h.

C. Western blot analysis of phosphorylated CREB (Ser133) and TRIM28 (Ser473) in 4-week-old mice treated with PBS or ACTH for 30 minutes. Graphs represent phosphorylated form over total form

D. Coimmunofluorescent labelling of GFP (green) with CYP21 (purple) or DAB2 (blue) on WT, $Senp2^{cKO}$, $Prkar1a^{cKO}$ or double knock-out adrenals.

E. Plasmatic concentration of corticosterone in 4-week-old WT, $Senp2^{cKO}$, $Prkar1a^{cKO}$ or double knock-out male and female mice

F. Plasmatic concentration of ACTH in 4-week-old WT, $Senp2^{cKO}$, $Prkar1a^{cKO}$ or double knock-out male and female mice

G. PKA kinase activity measurements in WT and $Senp2^{cKO}$ 4-week-old adrenals in presence or absence of 5µM SUMO vinyl sufone

H. Western blot analysis of global SUMOylation and PKA catalytic subunits protein accumulation 4-week-old adrenals from WT and $Senp2^{cKO}$ mice

that consequences of *Senp2* loss, including the excess of SUMOylation, had a dominant impact on the zF homeostasis over PKA constitutive activation. Then, we explored endocrine activity of double KO mice. Although plasma corticosterone dosage showed no differences among the four genotypes, plasma ACTH concentrations were elevated in $Senp2^{cKO}$ and reduced in $Prkar1a^{cKO}$, consistent with the corresponding associated disorders *i.e.* glucocorticoid deficiency and ACTH-independent glucocorticoid excess, respectively (Figure 3.E.F.). By contrast, *Senp2-Prkar1a* double ablation restored ACTH levels to control values. This strongly suggested that the lack of *Senp2* resulted, among other things, in the repression of PKA catalytic activity that the deletion of RIα regulatory subunits could partially overcome. Indeed, PKA kinase activity was decreased by 30% in $Senp2^{cKO}$ adrenal extracts compared to WT without affecting Cαβ protein levels (Figure 3.G.H.). To test a possible direct repressive effect of SUMOylation, we measured kinase activity in the presence of a mix of SUMO1/2 modified with vinyl sulfone (SUMOs-VS) acting as specific trap and potent inhibitors of SENPs SUMO proteases present in the extracts[28]. Under these conditions enhancing SUMOylation in adrenal extracts, PKA kinase activity was further decreased in $Senp2^{cKO}$, reaching a 50% inhibition (Figure 3.G.H.). Together, these results present SENP2 as a mandatory actor of proper ACTH response acting most likely by limiting repressive action of SUMOylation on the catalytic activity of the PKA holoenzyme.

Senp2 is necessary for the acquisition of zF identity

Based on the blunted response to ACTH, we decided to assess the differentiation status of the zF in $Senp2^{cKO}$ mice. We took advantage of cortical cells' capacity to escape recombination to compare the intensity of differentiation markers in neighbouring cells, differing only by their recombination status. We performed triple staining for GFP, used as a proxy of *Senp2* recombination, with DAB2 and AKR1B7 labelling zG and zF, respectively. We observed a consistent lower AKR1B7 staining intensity in GFP-positive cells, indicating that loss of *Senp2* hinders cells from expressing zF markers compared to neighbouring GFP-negative cells (Figures 4.A.B. & S4.A.). RT-qPCR analysis revealed an increased accumulation of progenitors' markers and higher number of NR2F2-positive capsular cells in males (Figure S4.B.C.) implying a default in cortical cell turnover which, together with the downregulated AKR1B7 expression, suggests a block in centripetal differentiation. This hypothesis was further supported by an increased proportion of cells coexpressing DAB2 and AKR1B7 in the cortex of $Senp2^{cKO}$, suggesting altered zG to zF transdifferentiation (Figure 4.C.). To examine this hypothesis, we performed functional lineage tracing analysis of *Senp2*-deficient cells using mTmG reporter mice and AS^{Cre} driver[2], which allowed to delete *Senp2* in zG cells after birth ($AS^{Cre}/+::Senp2^{fl/fl}::R26R^{mTmG/mTmG}$). This Cre driver enabled to assess cortex cellular turnover through the percentage of GFP-stained cells progressing centripetally. As previously shown[7,29], complete cortical cell took around 12 weeks in female and 40 weeks in male WT mice (Figure 4.D.). Interestingly, whereas GFP immunostaining marked the first third of the cortex (zG and upper zF) in 4 weeks WT females, GFP staining was confined to the zG and some rare stripes projecting into the zF in $AS^{Cre}/+$ $Senp2^{cKO}$ littermates (Figure 4.E.).

To accelerate lineage tracing, we mated Cre homozygosity, and thus deleted the Aldosterone

Synthase gene ($AS^{Cre/Cre}$::$Senp2^{fl/fl}$ ::$R26R^{mTmG/mTmG}$). Consistent with previous reports[2], this enhanced trophic drive through renin-angiotensin signalling, and increased recombination rate, leading to almost full recombination cortex by 4 weeks of age in $AS^{Cre/Cre}$ *Senp2* heterozygous female adrenal. In sharp contrast, GFP staining was almost confined to the zG in $AS^{Cre/Cre}$ $Senp2^{cKO}$ even though the zG was slightly expanded because of trophic stimulation by angiotensin (Figure 4.E.). A similar phenotype was observed in $AS^{Cre/+}$ $Senp2^{cKO}$ at 40 weeks of age with a recombined zF consisting of scattered stripes of GFP-positive cells (Figure 4.E.). We next quantified AKR1B7 protein accumulation in zF cells of $AS^{Cre/+}$ $Senp2^{cKO}$ of 40 weeks of age and again observed lower AKR1B7 staining in GFP-positive than in GFP-negative cells (GFP- 95% CI [6887;7164] AU, GFP+95% CI [5427;5582] AU, *P*-value = 10^{-16}) (Figure 4.F.G.). In contrast with *Sf1-Cre* mediated inactivation of *Senp2*, AS^{Cre} mediated deletion did not alter adrenal weight at 24 weeks of age (Figure 4.H.). However, when ACTH responsiveness was assessed over time, plasma corticosterone peaked 2 hours after ACTH treatment in WT, whereas the response was slower in $AS^{Cre/+}$ $Senp2^{cKO}$ and never reached statistical threshold (Figure 4.I.). This shows that even in the absence of adrenal hypoplasia, *Senp2* ablation results in a block of zF transdifferentiation from zG cells. This causes incomplete zF differentiation in recombined cells and allows competitive selection of non-recombined cells, which cannot completely overcome the endocrine phenotype.

Senp2 deficient cells undergo apoptosis associated with DRP1 phosphorylation

We next examined the cellular mechanisms underlying the development of zF atrophy in $Senp2^{cKO}$ mice, by analysing the proliferation/apoptosis balance. The cortical proliferation index determined by scoring the number of Ki67- or BrdU-positive cells ruled out the contribution of a decreased proliferation rate to the hypoplastic phenotype, but rather showed a trend toward increased cell division in mutant adrenals (Figure S5.A.B.). Nonetheless, cleaved caspase-3 staining showed that the numbers of cells undergoing apoptosis was dramatically increased in $Senp2^{cKO}$ adrenals at 4 and 8 weeks of age in both sexes (Figure 5.A.). Whereas, according to the standard model, apoptosis is normally found at the corticomedullary junction (where adrenal cells die after centripetal migration[30]), in the $Senp2^{cKO}$ cortex, apoptosis occurred prematurely at the border between the zG and zF (Figure 5.A.).

DRP1 (Dynamin Related Protein 1) is considered the primary driver of mitochondrial fission and mitochondrial-dependant cell death[31,32]. Phosphorylation of DRP1 on Ser616 activates mitochondrial fission while that on Ser637 prevents the fission. The dysregulation of DRP1 phosphorylations on these two residues will result in imbalanced mitochondrial fission/fusion, a major cause of apoptotic cell death. Phosphorylation on Ser637 particularly raised our attention since it is catalysed by PKA[33]. Besides its participation to inhibition of mitochondrial fission, studies have shown that phosphorylated DRP1-Ser637 promotes steroidogenesis in Leydig cells[34] and *corpus luteum*[35]. To assess the impact of ACTH/PKA on DRP1 activity in adrenal glands, we performed western blotting of DRP1 and its Ser637 phosphorylated form in WT or $Senp2^{cKO}$ adrenal treated with vehicle or ACTH for 30 min. We found no difference in total or phosphorylated DRP1 in vehicle treated mice. In constrast, ACTH

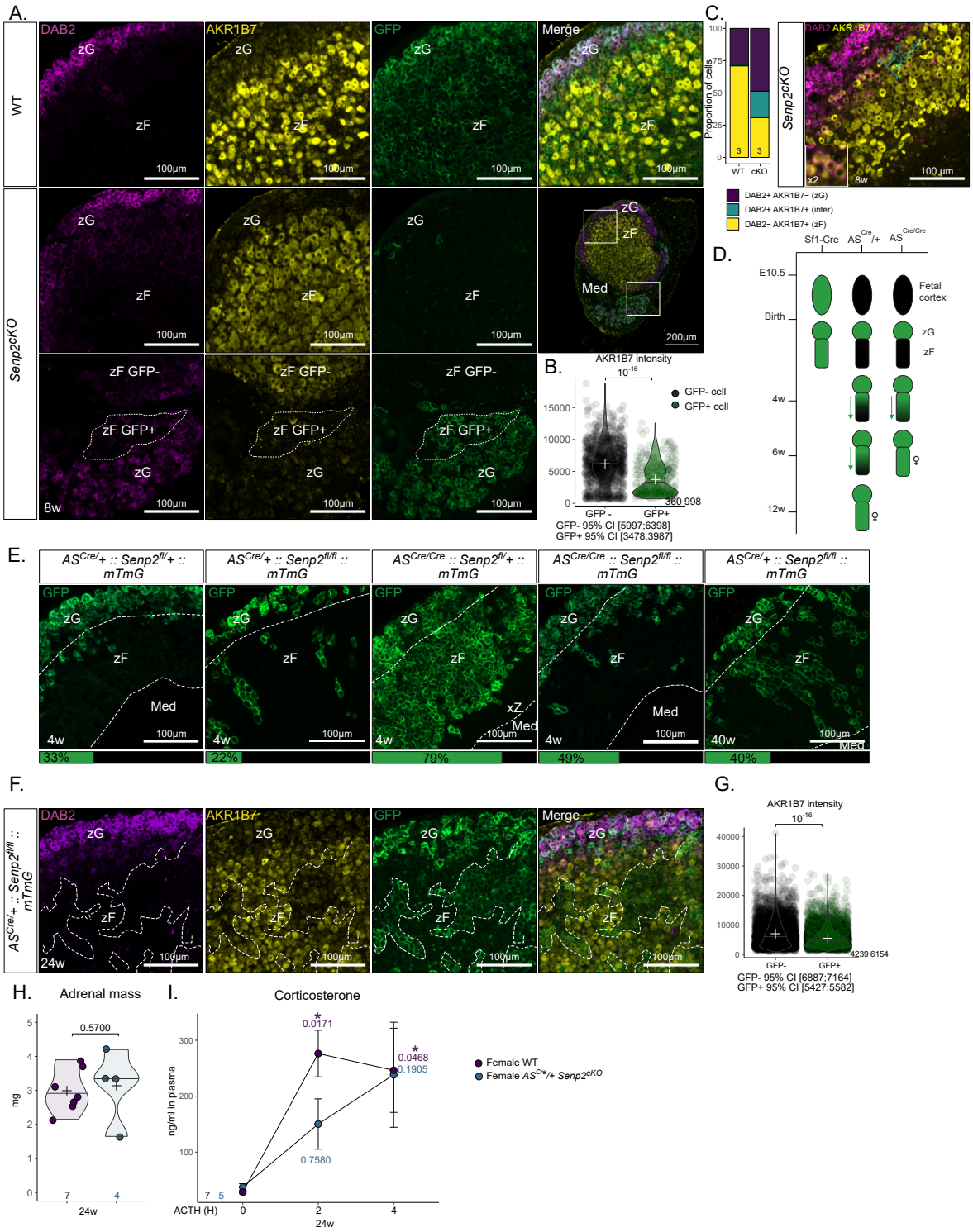

Figure 4: ***Senp2* ablation prevents proper zF differentiation**

A. Coimmunofluorescence labelling of AKR1B7 (yellow), GFP (green) and Disabled2/DAB2 (purple) on 8-week-old WT and $Senp2^{cKO}$ male adrenals

B. Quantification of AKR1B7 intensity in GFP+ and GFP- $Senp2^{cKO}$ male adrenal cells

C. Quantification and representative image of cells expressing DAB2 (purple), AKR1B7 (yellow) or both (blue) in WT and $Senp2^{cKO}$ 8-week-old adrenals

D. Scheme representing the differences in recombination kinetics between cre drivers used in genetic models

E. Immunofluorescence labelling with mean percentage of GFP-positive cells in 4w and 40w cortex

F. Coimmunofluorescence labelling of AKR1B7 (yellow), GFP (green) and Disabled2/DAB2 (purple) on female 24-week-old $AS^{Cre}/+$ $Senp2^{cKO}$ adrenals

G. Quantification of AKR1B7 intensity in GFP+ and GFP- 24-week-old $AS^{Cre}/+$ $Senp2^{cKO}$ adrenal cells

H. Mean adrenal mass of 24-week-old female $AS^{Cre}/+$ *Senp2* and WT

I. Kinetics of ACTH response of 24-week-old female $AS^{Cre}/+$ *Senp2* and WT. *P*-values represent difference between samples from the same mice before treatment compared to after 2 hours or after 4 hours of treatment.

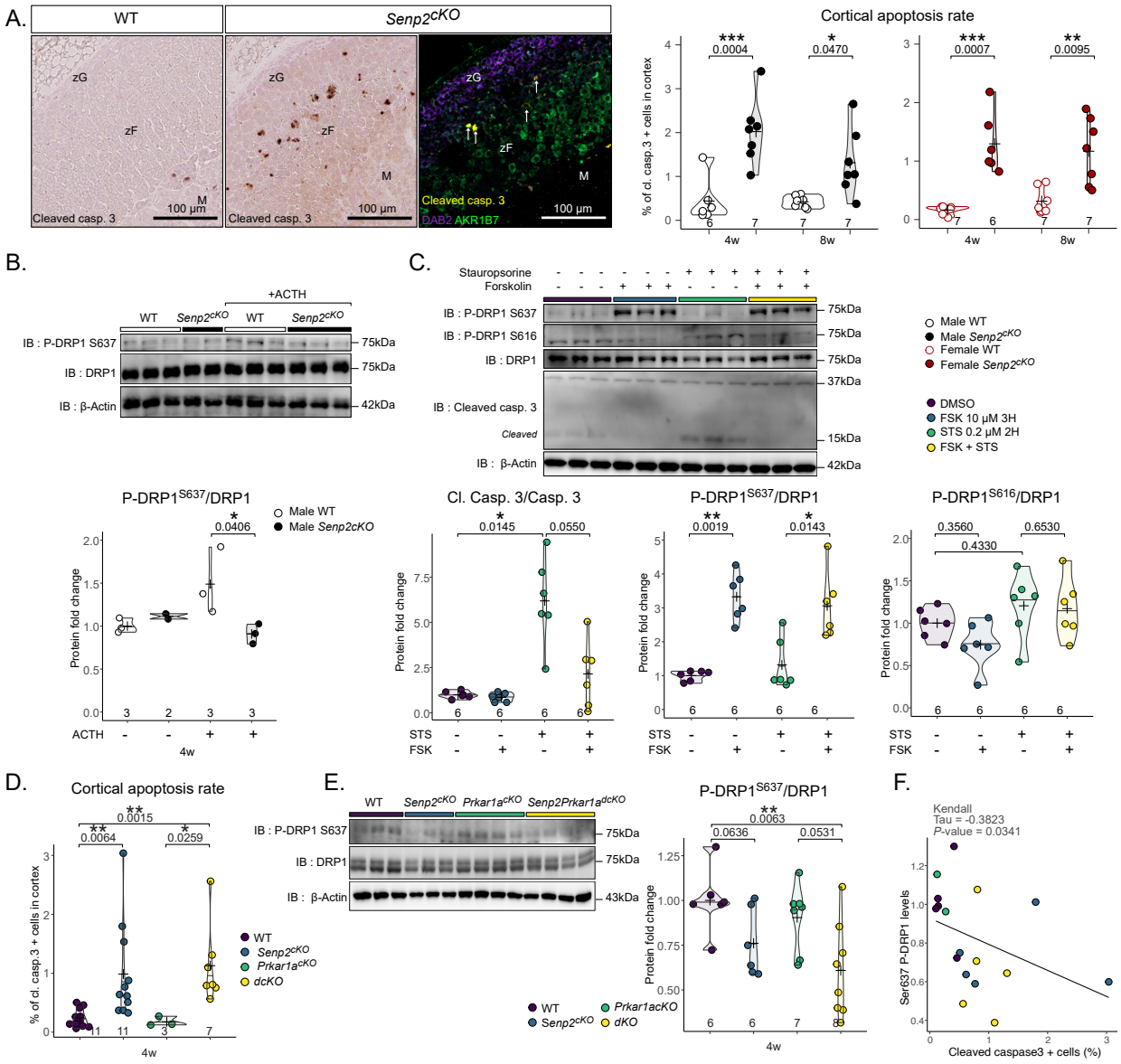

Figure 5: ***Senp2* loss triggers apoptosis at the zG-zF boundary**

A. Representative image of cleaved caspase-3 immunostaining and immunofluorescence labelling of cleaved caspase-3 (yellow), zG marker Disabled2/DAB2 (purple) and zF marker AKR1B7 (green). Quantification of apoptosis in WT and cKO through measurement of the percentage of cells positive for cleaved caspase3 at 4 and 8 weeks of age

B. Western blot analysis of S637 phosphorylated and total DRP1 in adrenal after 30 minutes ACTH I.P. treatment of WT and $Senp2^{cKO}$ male mice

C. Western blot analysis of phosphorylated and total DRP1 in cells treated with DMSO, Forskolin (10 µM) and/or Staurosporine (0.2 µM).

D. Quantification of cleaved caspase-3 positive cells in the cortex (E) of WT, $Senp2^{cKO}$, $Prkar1a^{cKO}$ and double knock-out male adrenals

E. Western blot analysis of S637 phosphorylated and total DRP1 in the cortex (E) of WT, $Senp2^{cKO}$, $Prkar1a^{cKO}$ and double knock-out males adrenals

F. Correlation plot between Ser637 DRP1 phosphorylation and proportion of cleaved caspase-3 positive cells in the adrenal cortex across genotypes

treatment induced DRP1 Ser637 phosphorylation solely in WT mice whereas this response was abolished in $Senp2^{cKO}$ adrenals (Figure 5.B.).

We then took an *in vitro* approach to determine whether PKA-induced changes in DRP1

phosphorylation were involved in the apoptotic response of adrenocortical cells. The *fasciculata*-like ATC7 cells[36] were treated with forskolin (FSK), a pharmacological activator of PKA (through increased cAMP cellular levels), one hour before a 2 hours-incubation with the proapoptotic drug staurosporine (STS). As expected, FSK alone resulted in increased Ser637 phosphorylation of DRP1, while STS alone induced caspase-3 cleavage. When combined, FSK limited STS-driven apoptosis, as depicted by the reduced accumulation of cleaved caspase-3 (Figure 5.C.). Of note, Ser616 proapoptotic phosphorylation of DRP1 showed a trend to be regulated in the exact opposite way to Ser637 (Figure 5.C.). To specifically assess the contribution of DRP1 in STS-induced apoptosis, we pretreated cells with the DRP1 specific inhibitor (Mdivi-1) before inducing apoptosis with STS[37]. Similar to FSK, pretreatment with Mdivi-1 resulted in protection against apoptosis as shown by reduced accumulation of cleaved caspase-3 (Figure S5.C.). Consistently *in vivo*, we observed an inverse correlation (τ = -0.3823, P-value = 0.0341) between cortical apoptosis rate and DRP1 Ser637 phosphorylation in *Senp2*, *Prkar1a* single and double knock-outs (Figure 5.D.E.F S5.D). Altogether, these results strongly suggest that increased apoptosis seen at the zG-zF boundary in $Senp2^{cKO}$ adrenals results from a deficient ability of ACTH/PKA signalling to properly phosphorylate DRP1 Ser637.

Senp2 deficiency leads to β-catenin hyperSUMOylation and mild activation of WNT pathway

To unravel new SUMOylation-sensitive pathways that could explain further the adrenal insufficiency of mice lacking SUMO protease SENP2, we performed bulk RNA sequencing on four-week-old male and female WT and $Senp2^{cKO}$. We found 1337 genes to be differentially expressed in male (1115 up and 222 down) and 1235 in female (960 up and 275 down) (Figure 6.A.B.). Unsupervised clustering and principal component analysis discriminated samples based on genotype but not on sex (Figure S6.A.B.), implying that at 4 weeks of age, sex has a low impact on gene transcription. Since most of the genes were co-regulated in males and females, we chose to focus on these subsets of genes. We performed Gene Ontology (GO) functional enrichment analysis on upregulated or downregulated genes in $Senp2^{cKO}$ adrenals of both sexes (Figure 6.C.). The top GO terms associated with the upregulated genes were linked to neuron cells and function, which may be due to over representation of medullar chromaffin cells resulting from cortical hypoplasia. Pathways related to steroid processing were enriched in downregulated genes, consistent with the endocrine deficiency phenotype of $Senp2^{cKO}$ mice.

We performed Get Set Enrichment Analysis (GSEA) on the Kyoto Encyclopedia of Genes and Genomes (KEGG) database and selected only the enriched pathways that were present in both males and females (Figure 6.D.). This confirmed negative enrichment of the gene signature for steroid hormone biosynthesis pathway, in accordance with GO analysis and hormonal insufficiency characterised in $Senp2^{cKO}$ mice (Figure 2.). Moreover, we found negative enrichment of signatures associated with nucleotide excision repair, aminoacyl tRNA biosynthesis, ribosome, pyrimidine metabolism and spliceosome, indicating that *Senp2* loss in the adrenal cortex altered basic cellular processes known to be regulated by SUMOylation[12].

Interestingly, among the positively enriched pathways, WNT signalling caught our attention as it is mandatory for adrenocortical maintenance and proper zonation[38–40] (Figure 6.D.E.)

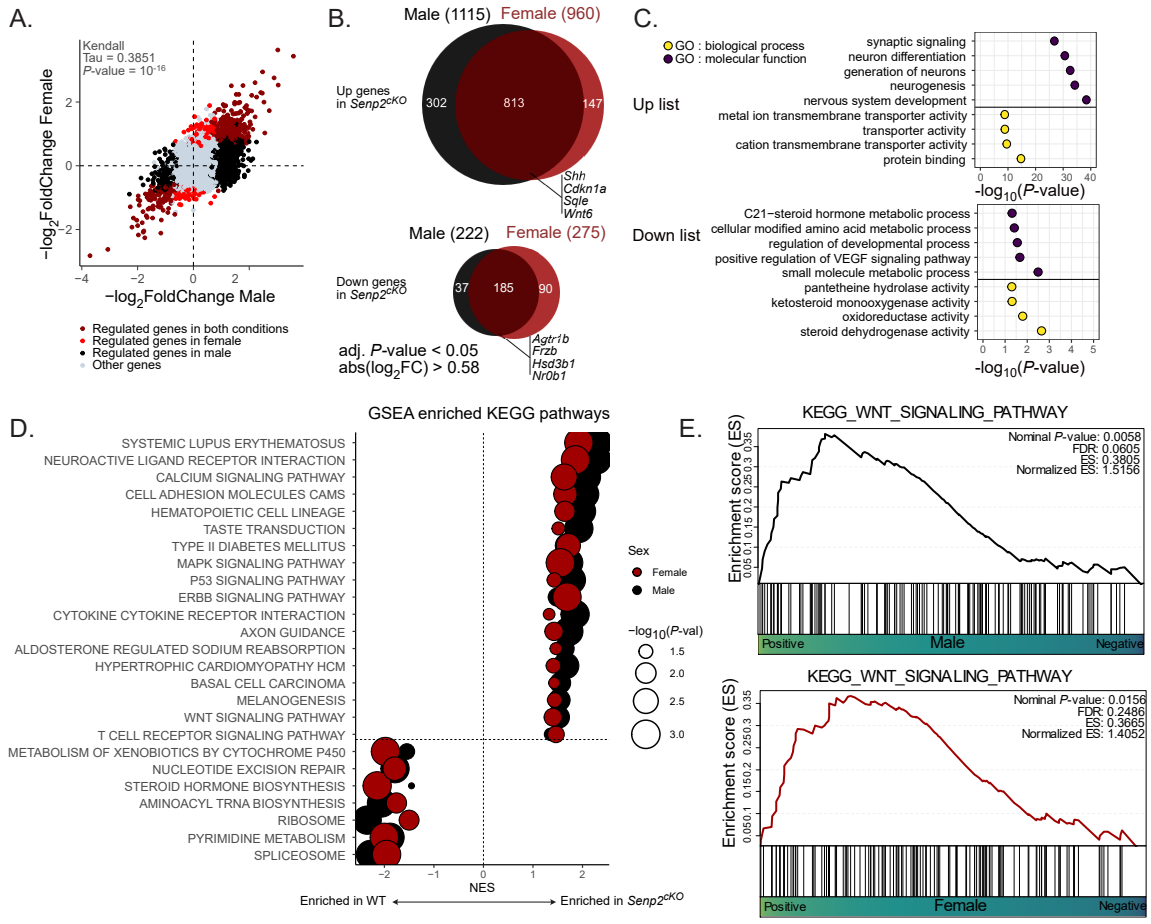

Figure 6: **RNA-seq analysis of male and female *Senp2*^{cKO} adrenals**
A. Scatter plot showing the correlation between dysregulated genes (adjusted P-value < 0.05 and absolute $\log_2$ fold change > 0.58) in male and female *Senp2*^{cKO} adrenals at 4 weeks of age
B. Euler diagrams illustrating the commonly up or downregulated genes in both sexes *Senp2*^{cKO} adrenals at 4 weeks of age
C. Top GO terms from Gene Ontology functional enrichment analysis based on the up or downregulated genes lists
D. Gene set enrichment analysis (GSEA) pathways from the KEGG database that are commonly affected in male and female *Senp2*^{cKO} adrenals
E. Gene set enrichment analysis (GSEA) plots of WNT pathway on male and female WT versus *Senp2*^{cKO} adrenals

Based on RNA-Seq analyses and given that SENP2 has first been described as a negative regulator of β-catenin[41–43], we sought out to see if the WNT/β-catenin pathway was altered in *Senp2*^{cKO} adrenals. We evaluated the activation of the pathway by running RT-qPCR on its target genes. At 24 weeks of age, we observed a consistent ~1.5 fold induction of *Axin2*, *Lef1*, *Apcdd1* and *Ccdc80* in the adrenals of *Senp2*^{cKO} females, whereas in mutant males, only *Ccdc80* was upregulated by about 3 fold (Figure 7.A.). To gain more insight into the modulation of the WNT signalling pathway, we extracted expression levels of 48 WNT target genes from RNA-seq data (Figure 7.B.). Among these genes, 31 were upregulated mainly in males *Senp2*^{cKO} and 7 mainly in females while 10 genes were downregulated in both sexes.

We next carried out immunostaining on adrenal sections that revealed a nuclear localisa-

tion of non-phospho (active) β-catenin specifically in the inner cortex of mutant adrenals regardless of sex (Figure 7.C. top). Co-staining of total β-catenin with zF marker AKR1B7 confirmed zF identity of these cells, which were also GFP-positive and hence, had been targeted by Cre recombination (Figure 7.C. bottom).

Given that β-catenin can be SUMOylated by both SUMO1[44] and SUMO2/3[45], we hypothesised that it was SUMOylated in the adrenal cortex. We performed immunoprecipitation of both SUMO1 or SUMO2/3 and blotted β-catenin. We observed a doublet between 120 and 150 kDa for SUMO2/3 consistent with a previous report[45] but no evidence for significant SUMO1 conjugation (Figure 7.D.). To evaluate if β-catenin SUMO2/3-ylation was affected upon *Senp2* deletion, we immunoprecipitated β-catenin and blotted SUMO2/3. Although we did not see any difference in the amount of SUMOylated β-catenin, the accumulation of its native form was reduced in mutant adrenals whereas global SUMOylation by SUMO2/3 was unchanged (Figure 7.E.). Reciprocally, by immunoprecipitating SUMO2/3 and blotting β-catenin, we observed a slight but reproducible accumulation of SUMOylated β-catenin compared to native form (Figure 7.F.). To confirm this increase in β-catenin SUMO2/3-ylation, we used Proximity Ligation Assay (PLA) which enables to visualise *in situ* the close proximity of two proteins (Figure 7.G.). As a negative control, we first ran PLA between β-catenin and GATA6, a transcription factor present in the nucleus of all adrenocortical cells and which is not known to interact with β-catenin. As expected, there were no *foci* of β-catenin/GATA6 interaction in adrenal sections of all genotypes. In contrast, PLA between β-catenin and SUMO2/3 showed specific *foci* in the zG with similar density in both genotypes. However, in the zF of $Senp2^{cKO}$, there was an increase in cells containing 2 or more β-catenin/SUMO2/3 dots per nucleus (Figure 7.G.).

In conclusion, loss of SENP2 leads to ectopic nuclear accumulation of β-catenin in the zF associated with its increased conjugation to SUMO2/3. This accumulation is correlated with a mild activation of WNT pathway targeting genes in a partially sexually dimorphic pattern.

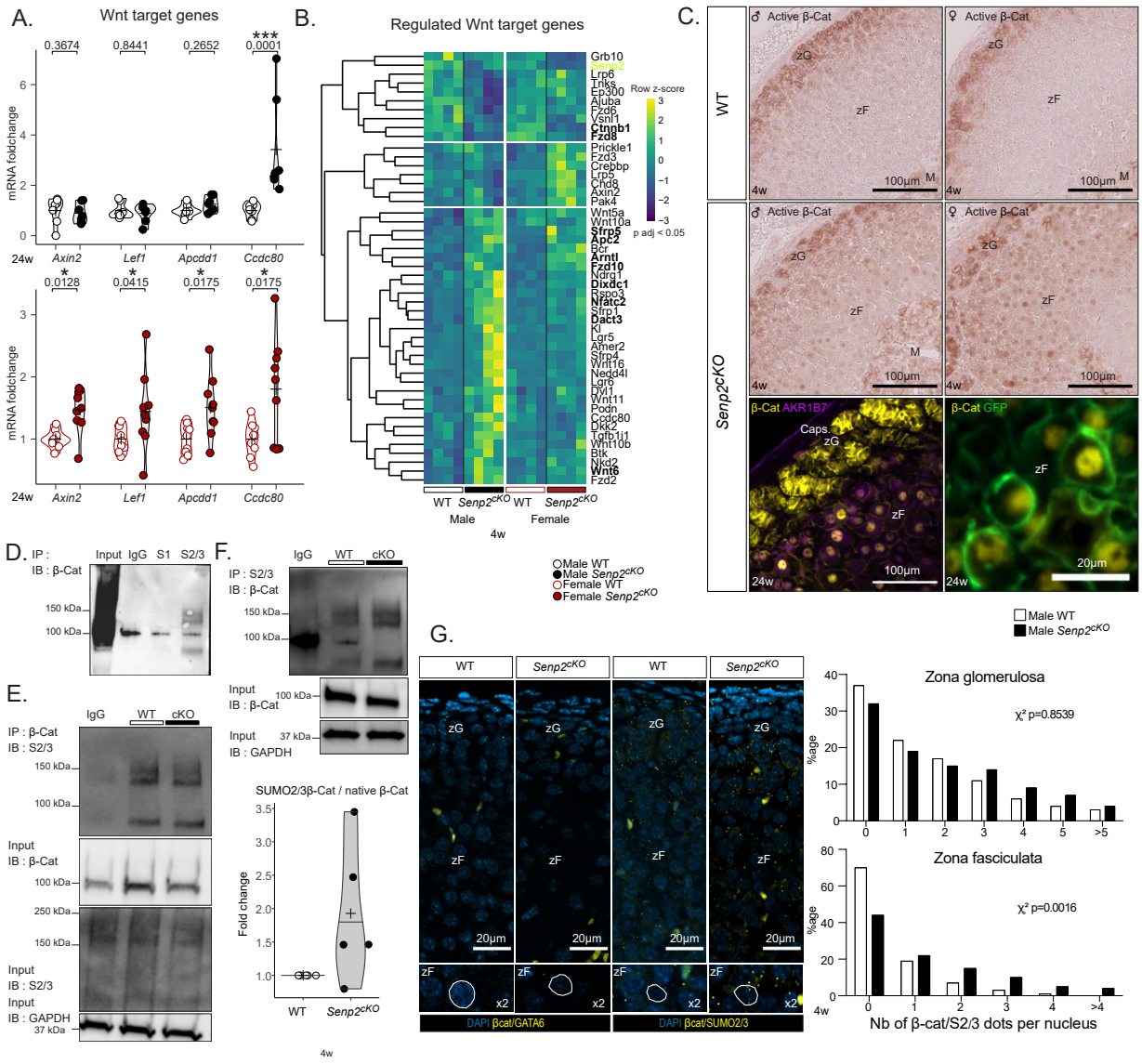

Figure 7: ***Senp2* loss promotes β-catenin SUMOylation and activates the WNT signalling pathway**

A. qPCR analysis of β-catenin target genes *Axin2*, *Lef1*, *Apcdd1* and *Ccdc80* mRNA accumulation in 24-week-old WT and $Senp2^{cKO}$ mice.

B. Heatmap of dysregulated WNT target genes in $Senp2^{cKO}$ male or female adrenals RNA-seq (adjusted P-value < 0.05). Commonly dysregulated genes in males and females are represented in bold characters.

C. Top : Immunohistochemistry analysis of active (non-phospho) β-catenin on WT and $Senp2^{cKO}$ male (left) and female (right) adrenals.

Bottom : immunofluorescence staining of β-catenin (yellow) with zF marker AKR1B7 (purple) and GFP (green).

D. Immunoprecipitation assay depicting the interaction between β-catenin and SUMO1 or SUMO2/3 in WT adrenals.

E. & F. Immunoprecipitation assay depicting the interaction between β-catenin and SUMO2/3 in adrenals of 4-week-old WT and $Senp2^{cKO}$ male mice. Extracts were immunoprecipated with β-catenin (D) or SUMO2/3 antibodies (E). SUMOylated β-catenin was quantified relative to its native form.

G. Proximity ligation assay (PLA) of β-catenin and GATA6 (negative control) or β-catenin and SUMO2/3 in nuclei of 4-week-old WT and $Senp2^{cKO}$ male mice's adrenals. Histograms represent proportion of cells in each zone containing the specified number of dots per nucleus of WT and $Senp2^{cKO}$ male adrenals. n = 6 per genotype

Ca, capsule; zG, *zona glomerulosa*; zF, *zona fasciculata*.

Discussion

We have previously established that the overall SUMOylation of proteins in the adrenal cortex displays two remarkable properties: it gradually decreases as the centripetal transdifferentiation of zG cells into zF cells progresses and it is acutely downregulated by stress through ACTH/PKA signalling[20]. The present study was initiated to address the hypothesis that this posttranslational mechanism involved in the cellular response to various environmental stressors[46] may be an integral part of the adrenal gland's toolbox to produce steroid hormones critical for body homeostasis and stress adaptation. Adrenal-specific KO mouse models of SENP2 deSUMOylase and of PKA regulators established that this is indeed the case. Foetal or postnatal SENP2 dependent deSUMOylation is necessary for initial zF differentiation, its maintenance thoughout life and for ACTH/PKA-stimulated glucocorticoid production. As a result, foetal or postnatal deletion of *Senp2* in adrenal steroidogenic cells causes postnatal hypoplasia limited to the zF or incomplete zF formation respectively, which can lead to isolated glucocorticoid deficiency. This selective atrophy and associated endocrine deficit result both from a blockage of zonal transdifferentiation preventing the switch from zG to zF identity, and from a repression of ACTH/PKA responsiveness. Interestingly, overt corticosterone deficiency is only measurable in males at 4 weeks of age, even though ACTH levels are higher at all ages tested in both genders. This implies that a subclinical deficiency is permanently established in the mutants, despite setting up compensation. This compensation to maintain physiological plasma glucocorticoid levels, which occurs in both sexes but with delay in males, most likely relies on the emergence of a population of cells that has escaped recombination and helps the mutant cortex to overcome zF atrophy. Indeed, their hypertrophy indicates that they are overreacting to the high levels of circulating ACTH, to compensate for the lack of corticosterone due to the dramatic atrophy of the *Senp2*-deficient zF cell population.

We hypothesise that steroidogenic progenitor cells, which do not express the Cre recombinase for a still unknown reason, must gain a selective advantage over *Senp2*-deficient cells, either by being able to proliferate more or by being less prone to death upon differentiation. Similar observations have been made in adrenals following SF-1 loss driven by AS^{Cre2} or *Cyp11a1-Cre*[47], where a majority of cells escaped recombination. How cells manage to express a protein but not the Cre while both genes depend on the same promoter is still unknown. One possibility could be methylation of the promoter. For instance, *Ins1-Cre* transgene is shown to be a poor quality driver to target β cells in the pancreas as its expression is silenced by *de novo* methylation even though *Ins1* gene is normally expressed[48]. In any case, the triggering of a compensatory mechanism underlines the absolute necessity of maintaining *Senp2* expression (and thus the possibility of reducing SUMOylation), in order to build a functional *zona Fasciculata* to maintain the individual's ability to adapt to stress.

The fact that *Senp2*-deficiency preferentially affects the zF while being expressed in all cortical areas[49] can be explained by two non-mutually exclusive mechanisms. First, the zG already harbours high levels of nuclear SUMOylation compared to the zF[20], therefore the expected increase in SUMOylation conjugates consecutive to lowered deconjugase pools will preferentially affect hypoSUMOylated regions. Moreover, we showed that SENP2 loss alters the PKA/WNT balance toward WNT signalling. The latter being already highly active in

the zG[4,6,38], it is not surprising to find an altered phenotype only in the zF where WNT/β-catenin signalling is naturally repressed[9]. The second reason is that low SUMOylation seems to be a prerequisite for adequate PKA signalling. Indeed, in our model, ACTH response is blunted and the zF atrophy phenotype is reminiscent, at least partially, of mouse models lacking ACTH receptor and its co-receptor *i.e.* *Mc2r*$^{-/-}$ or *Mrap*$^{-/-}$ whole-body knock-outs[50,51]. Although various mechanisms could be simultaneously affected and remain to be explored, there are converging pieces of evidence that SENP2 deletion-dependant SUMOylation alters PKA responsiveness. Indeed, first, our data show that SENP2 deletion decreases overall PKA activity in the adrenal glands and prevents the phosphorylation of specific targets (CREB^{Ser133}, DRP1^{Ser637}, TRIM28^{Ser473}). Secondly, since *Senp2*^{cKO} phenotype is not rescued by concomitant deletion of PKA regulatory subunit (*Prkar1a*), it is very likely that SENP2 loss directly affects the PKA catalytic subunits function. This is in line with 1) the presence of conserved K169 lysine in the major subunits (PRKACA and PRKACB) amino acid sequence, predicted as a SUMO consensus motif (ψKxD/E where ψ is a hydrophobic residue) and 2) the decreased PKA activity caused by SUMO vinyl sulfone derivatives (figure 3.G.H.). Further studies will assess the SUMOylation of the catalytic subunits and their potential in fine-tuning PKA kinase activity.

SENP2 has first been described as a negative regulator of β-catenin stability[43] but this effect was independent of SUMOylation. Our model showed increased β-catenin SUMO2/3ylation along with ectopic nuclear β-catenin localisation associated with a gene signature indicative of the canonical WNT signalling. Similar observations have been reported following direct SUMOy2/3lation of β-catenin in mammary epithelial cells[45] or SUMOylation of TBL1/TBLR1 that in turn increased chromatin recruitment of β-catenin and its oncogenic activity in colon cancer[52]. However, the picture is not as clear since β-catenin SUMO2/3ylation can trigger its degradation in vascular smooth muscle cells[53] or prevent it in mammary epithelial cells[45]. Targeting gain-of-function mutation of β-catenin in aldosterone-synthase expressing cells caused hyperplasia by blocking *glomerulosa* cells transdifferentiation into *fasciculata* cells[3]. However, in contrast to *Senp2*^{cKO} mice, zF cells never became atrophic in β-catenin gain-of-function. It was thus proposed that when physiological transdifferentiation is unachievable, the zF can be maintained by an alternative cellular pathway involving progenitor cells that bypass the zG state[2]. Here, we report the first occurrence of β-catenin SUMOylation associated with its nuclear translocation which takes place ectopically in *Senp2*-deficient zF. This leads to moderate WNT target genes activation and together with blunted PKA activity, impairs acquisition of *fasciculata* identity. In this context where zG-to-zF zonal transdifferentiation is impaired, the deficit in PKA signalling alters the phosphorylation profile of the major mitochondrial fission GTPase, DRP1, leading to premature apoptosis of the neoformed mutant *fasciculata* cells, reinforcing the atrophy of the zone over time. The block in zonal transdifferentiation induced by zG-targeted stabilised β-catenin has been ascribed to increased rosette formation (the basal cellular organisation of zG cells forming flower-like structures) and/or impaired rosette resolution (the moment when zG cells exit the rosette to form a single column of cells typical of zF)[54]. Conversely, adrenal cortex lacking *Senp2* do not exhibit zG hyperplasia and thus should not display enhanced rosette formation. Our data indicate that mechanisms by which zG undergoes resolution during normal homeostatic turnover could

be controlled by SUMOylation. Identifying what targets of *Senp2*-dependent SUMOylation directly contribute to zG resolution and whether this is coupled to zF transdifferentiation will require extensive studies.

SUMOylation has already proven a role in adrenocortical development with the unSUMOylatable *SF-1*$^{2KR/2KR}$ model, which results in adrenal cells expressing gonadal markers[21]. In ovaries which share a common foetal origin with adrenals, SUMOylation by the E3 SUMO ligase activity of TRIM28, is essential for maintenance of granulosa cell fate at the expense of Sertoli-like identity[55], whereas SENP1 presence in stromal cells is necessary for proper oocyte maturation and ovulation[56]. From a broader perspective, our study belongs to a growing corpus of evidence associating SUMOylation with coordination of differentiation in different tissues and cell types such as white and brown adipose tissue[15,17,57], induced pluripotent stem cells[16], or intestine[18]. Seemingly counter-intuitively, the induction of the adrenal phenotype of *Senp2*^{cKO} mice does not rely on an overall increase in SUMO conjugates levels but rather on specific overSUMOylation of certain cell populations (Figure S1.I.J.) or substrates belonging to signalling pathways crucial for adrenal homeostasis. These findings are consistent with recent studies exploring the consequences of increased SUMOylation in the uterine stroma (by *Senp1* deletion) or decreased SUMOylation (by *Ubc9* haploinsufficiency) in the intestine of *Apc* mutant mice that showed strong phenotypes in the absence of global changes in visible SUMO conjugate levels[58,59]. This illustrates the great versatility of this posttranslational modification pathway. Changes in SUMOylation capacity can have specific effects *in vivo*, especially when targeted steps are catalysed by various members of the same enzymatic family, such as E3 SUMO-ligases or SUMO-specific proteases, which can therefore differ in their substrate specificity. With this in mind, we speculate that specific over-SUMOylated substrates produced in *Senp2*-deficient adrenals should result from the primary loss of the SUMO-protease. Their SUMOylation could be reinforced by the unrepressed (hypo-phosphorylated) E3 SUMO-ligase activity of TRIM28[60,61], secondary to the blunted ACTH/PKA signalling.

Overall, the present paper demonstrates that preventing deSUMOylation by adrenocortical specific SENP2 ablation induces zF hypoplasia associated with increased premature apoptosis along the lineage conversion zG-zF process, ultimately resulting in a blockage of the physiological differentiation process, translating to isolated glucocorticoid deficiency. This is linked to dysregulation of WNT/PKA balance in favour of WNT signalling. This shift highlights the central role of SUMOylation in physiological processes such as differentiation, tissue maintenance, and stress response. Furthermore, our data could broaden the scope of expected impacts of SUMOylation alterations to endocrine pathogenesis. Although pathogenic associations have been made with alterations in SUMO enzymes or substrates, direct causal links to pathologies have very rarely been established[13,62]. Our work suggests that genetic alterations leading to excessive SUMOylation could be associated with isolated glucocorticoid deficiency in patients.

Methods

Cell culture

Adrenocortical tumour cell line 7 (ATC7) cells were established from an adrenal tumour derived from a mouse expressing the Simian Virus 40 large T (SV40 T) antigen under the control of the aldo-keto reductase 1b7 (*Akr1b7*) gene promoter specific to the adrenal cortex[36,63]. Cells were cultured on poly-D-lysine–coated 10 cm cell culture dishes (MilliporeSigma, Burlington, MA) in a DMEM-F12 medium (Thermo Fisher Scientific, Waltham, MA) at 37°C in the presence of 5% CO2, insulin (10 mg/mL), transferrin (5.5 mg/mL), selenium (6.7 ng/mL) (Thermo Fisher Scientific), L-glutamine (2 mM), penicillin 0.1 U/mL), streptomycin (0.1 mg/mL), 2.5% horse serum, and 2.5% foetal calf serum. Cells were seeded in 12-well plates and cultures to subconfluence and then starved by replacing medium by serum-free medium the day before the addition of forskolin (Sigma-Aldrich), staurosporine (Sigma-Aldrich) or Mdivi-1 (Merck) at the times and concentrations indicated in the figure's legends.

Mice

Mice bred in-house and maintained on a mixed sv129-C57Bl/6 genetic background were housed on a 12-hour light/12-hour dark cycle (lights on at 7:00 am). Mice were fed normal, commercial rodent chow and provided with water *ad libitum*. After weaning, mice were kept in siblings with a maximum of 4 animals per cage.

Hormonal measurements

Mice were killed by decapitation around 8:30 am and blood was collected in vacuum blood collection tubes (VF-053STK, Terumo). For ACTH treatments mice were injected intraperitoneally with 0.05 mg/30g Synacthene (0.25 mg/mL, Novartis, Basel, Switzerland) 2 hours or 30 minutes prior the euthanasia. ACTH response kinetics in Figure4.I., was done with collection of the blood from the tail of the mice at 8 am, 10 am and 12 pm.

Corticosterone was measured from serum with ELISA kit (AR E-8100, LDN), ACTH was measured with Milliplex Map Kit (MPTMAG-49K, Millipore) and other steroids were measured by LC-MS/MS[64].

Histology and Proximity ligation assay

Adrenals were fixed in 4% PFA for 6 hours and embedded in paraffin. 5µm sections were deparaffinised and processed for H&E. For immunohistochemistry or immunofluorescence, deparaffinised slides were submerged in antigen retrieval buffer and microwaved for 8 minutes. After being rinsed with 1X PBS, they were blocked for an hour with 2.5% horse serum (Vector) and incubated overnight at 4°C with primary antibody. After rinsing, they were incubated with ImmPRESS polymer for 30 minutes at room temperature. HRP activity was detected with NOVAred (Vector) or Alexafluor (Thermo Fisher). Primary antibodies are listed in supplementary table S1.

For PLA, blocked slides were incubated overnight at 4°C with indicated antibodies followed by Duolink *in situ* PLA (Sigma-Aldrich) anti-mouse (minus) and anti-rabbit (plus) probes and detection reagents according to manufacturer's instructions.

Images were acquired with Zeiss Axioscan Z1 or Zeiss Imager M2 and analysed with QuPath software[65].

RT-qPCR

Adrenal glands were removed, flash frozen on dry ice, and RNA was extracted using RNeasy micro kit from QIAGEN. After reverse transcription, PCR reaction was conducted using SYBR qPCR Premix Ex Taq II Tli RNase H+ (TAKRR820W, Takara). Primer pairs are listed in supplementary table S2.

RNA-Seq

For each sex, adrenal gene expression profiles for four 4-week-old *Sf1-Cre/+::Senp2*$^{fl/fl}$ and four WT littermates were analysed using RNA-seq. RNA-sequencing, library generation and differential expression genes analysis were performed by the GenomEast platform (IGBMC, Illkirch, France).

Image analysis and base calling were performed using RTA 2.7.3 and bcl2fastq 2.17.1.14. Adapter dimer reads were removed using DimerRemover Reads were mapped onto the mm10 assembly of *Mus musculus* genome using STAR version 2.5.3a. Gene expression quantification was performed from uniquely aligned reads using htseq-count version 0.6.1p1. Read counts have been normalised across samples with the median-of-ratios method proposed by Anders and Huber. Differential expression have been implemented using the Bioconductor package DESeq2 version 1.16.1. Raw and processed data have been deposited in NCBI's GEO database (GSE193480).

Gene Set Enrichement Analysis was performed using the GSEA software[66] and plotted using the replotGSEA function from the Rtoolbox package (https://github.com/PeeperLab/Rtoolbox). Gene ontology analysis was performed using g:Profiler[67]. Data visualisation was carried out using R software (v4.1.0)[68], Pheatmap package was used for heatmaps, Vennerable for Euler diagrams and ggplot2 for plots. PCA analysis was produced on read counts matrix using prcomp function from the stats package and plotted using ggplot2.

Western blot and immunoprecipitation

Proteins were extracted from snap frozen adrenals in RIPA buffer (TRIS 25 mM, EDTA 1 mM, $MgCl_2$ 5 mM, NP40 1%, glycerol 10%, NaCl 150 mM supplemented extemporaneously with phosphatase inhibitors (1 mM Na_3VO_4, 0.5 mM NaF), protease inhibitors (Roche, Basel, Switzerland), and SUMO proteases inhibitor N-ethylmaleimide (MilliporeSigma) (3.13 mg/mL).

For western blot, thirty µg of total denatured proteins were loaded on 10% SDS-page gel, transferred on nitrocellulose and detected with primary antibodies (Supplementary table 2). Signals were quantified with ChemiDoc MP Imaging System camera system (Bio-Rad) and Image Lab software (Bio-Rad). Expression of phosphorylated or SUMOylated proteins was normalised to the expression of the corresponding unmodified protein.

Immunoprecipitation was carried out using Automag Solution (AdemTech). 500-1000 µg of total proteins were precleared with 50 µL of beads for 30 minutes at room temperature. 10 µL of antibodies (Supplementary table 2) were crosslinked with 50 µL of beads in 20 mM DMP for 30 minutes. Precleared samples were immunoprecipitated with crosslinked antibodies for 60 minutes at room temperature, washed thrice in RIPA buffer and eluted with 50 µL of 50 mM glycine pH3. pH was brought back to neutral with 1 µL of TRIS buffer pH9 and samples were denatured in Laemmli buffer (Bio-Rad) at 95°C for 5 minutes and loaded for SDS-PAGE.

PKA activity

Proteins were extracted from snap frozen adrenals in lysis buffer (MOPS 20 mM, Betaglycerol-phosphate 50 mM, NP40 1%, DTT 1 mM, EDTA 2 mM, EGTA 5 mM supplemented extemporaneously with phosphatase inhibitors (1 mM Na_3VO_4, 50 mM NaF), protease inhibitors (Roche, Basel, Switzerland). HA-SUMO vinyl sulfone (R&D Systems, Minneapolis, MN) was added for the SUMO-VS condition to the concentration of 5 µM for both SUMO1 and SUMO2.

10 µg of protein from 4-week-old adrenals were used for measurement with PKA kinase activity kit (ab139435, Abcam).

Statistics

Statistics were conducted using R language[68] and Comp3Moy function from sumo package (https://github.com/Damien-Dufour/sumo). Normality of populations distribution was assessed with Shapiro & Wilk test for n ∈ [7,5000] or otherwise Kolmogorof- Smirnov normality test.

If data followed a normal distribution, homoscedasticity was estimated with a Barlett test. To compare two populations, unpaired, two tailed t-test was used for normally distributed data with the same variance, Mann-Whitney for non normal distributions and Welch t-test for normally distributed data but with different variances. To compare three or more distributions : one way ANOVA for normally distributed samples with pairwise multiple t.tests or Kruskal-Wallis for non normally distributed samples with planned comparisons using Dunn's test to determine the genotype effect or the treatment effect

Crosses on the violin plots represent the mean and lines represent the median. Error bars in barplot represent the SD unless otherwise stated. The number of samples per condition is indicated at the bottom of each plot. Corticosterone response to ACTH in Figure 4.I. was analysed with paired 2 way ANOVA to compare the effect of treatment for each genotype. Correlations in Figure 5.F. and 6.A. have been conducted using cor.test function from stat package and Kendall method as distributions did not follow normality and contained ties.

Ethical approval declarations

Mouse experiments were conducted according to French and European directives for the use and care of animals for research purposes and were approved by the Comité d'Éthique pour l'Expérimentation Animale en Auvergne (project agreement #21152-2019061912052883), C2EA-02, at Institut National de Recherche pour l'Agriculture, l'Alimentation et l'Environnement, Research Centre Clermont-Theix, France (C2E2A).

Data availability

Sequencing data has been deposited in GEO with the accession code GSE193480. All other data that supports the findings of this study is provided in the article or supplementary

data. Source data is provided with this paper.

Code availability

All code for data cleaning and analysis associated with the current submission is available upon request.

Supplementary information

Acknowledgements

We thank K. Ouchen, S. Plantade, and P. Mazuel for animal care, A. Dehaze and J.P. Saru for their technical assistance, and Y. Renaud for management of the bioinformatic platform.

Authors' contributions

DD, TD, GB and AM designed research. DTB and ETH provided AS^{Cre}-expressing and *Senp2*-floxed mice, respectively. DD, ISB, MO, EP, JJW, JO, CL, AL, CSD, JCP and FRB performed experiments. DD and AM analysed data. DD and AM wrote the paper. GB, IT, DTB, PV and AMLM edited the paper.

Funding

This work was funded through institutional support from CNRS, INSERM, Université Clermont-Auvergne, the French government IDEX-ISITE initiative 16-IDEX-0001 (CAP 20-25), and grants from Ministère de l'Enseignement Supérieur, de la Recherche et de l'Innovation (to DD), Société Française d'Endocrinologie (to DD and AM), Fondation Association pour la Recherche sur le Cancer (to JW and JO), and Agence Nationale pour la Recherche (ANR-18-CE14-0012-02 Sex-Specs to AL and AM).

Competing interests

The authors declare no conflict of interest.

Supplementary figures

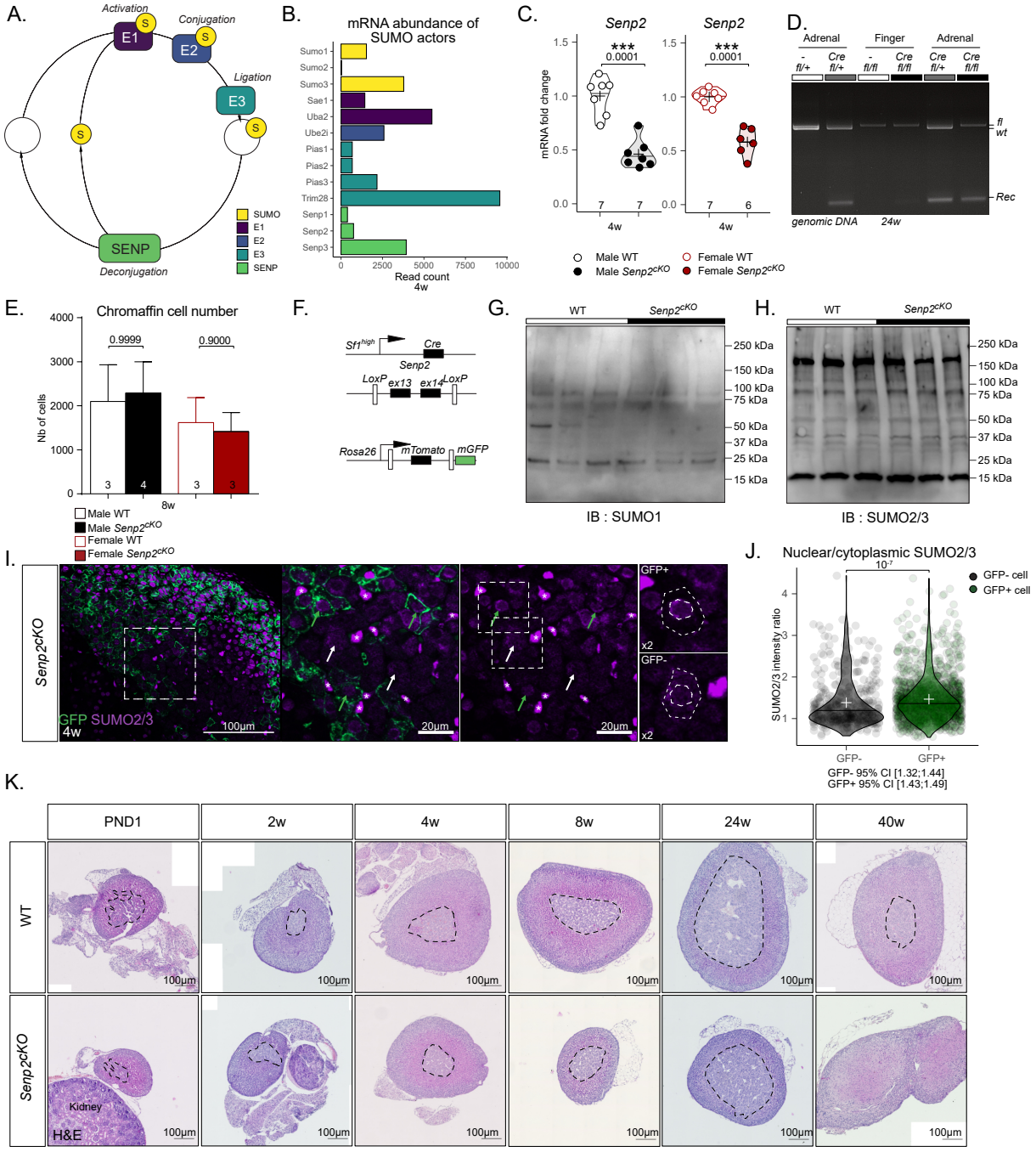

Fig.S 1: **Related to figure 1**

A. Schematic representation of the SUMOylation process

B. Relative abundance of the main actors of SUMOylation in the adrenal gland

C. qPCR analysis of *Senp2* mRNA accumulation in 4-week-old adrenals

D. Genomic PCR of *Senp2* gene showing specific recombination in *cKO* adrenals

E. 2D cell counting number in male and female medulla of WT and $Senp2^{cKO}$ mice

F. Scheme representing genetic model of $Senp2^{cKO}$ and reporter gene *Rosa26RmTmG*

G. Western blot analysis of SUMO1 in WT and $Senp2^{cKO}$ 4-week-old adrenals

H. Western blot analysis of SUMO2/3 in WT and $Senp2^{cKO}$ 4-week-old adrenals

I. Coimmunofluorescent labelling of GFP (green) and SUMO2/3 (purple) in $Senp2^{cKO}$ adrenal cortex at 4 weeks of age. Asterisks represent endothelial cells

J. Quantification of the ratio of nuclear vs cytoplasmic intensity of SUMO2/3 in GFP-negative cells vs GFP-positive cells in $Senp2^{cKO}$ adrenal cortex

K. Ontogenic analysis of adrenal morphology with H&E staining. Dotted lines represent the boundaries of the medulla.

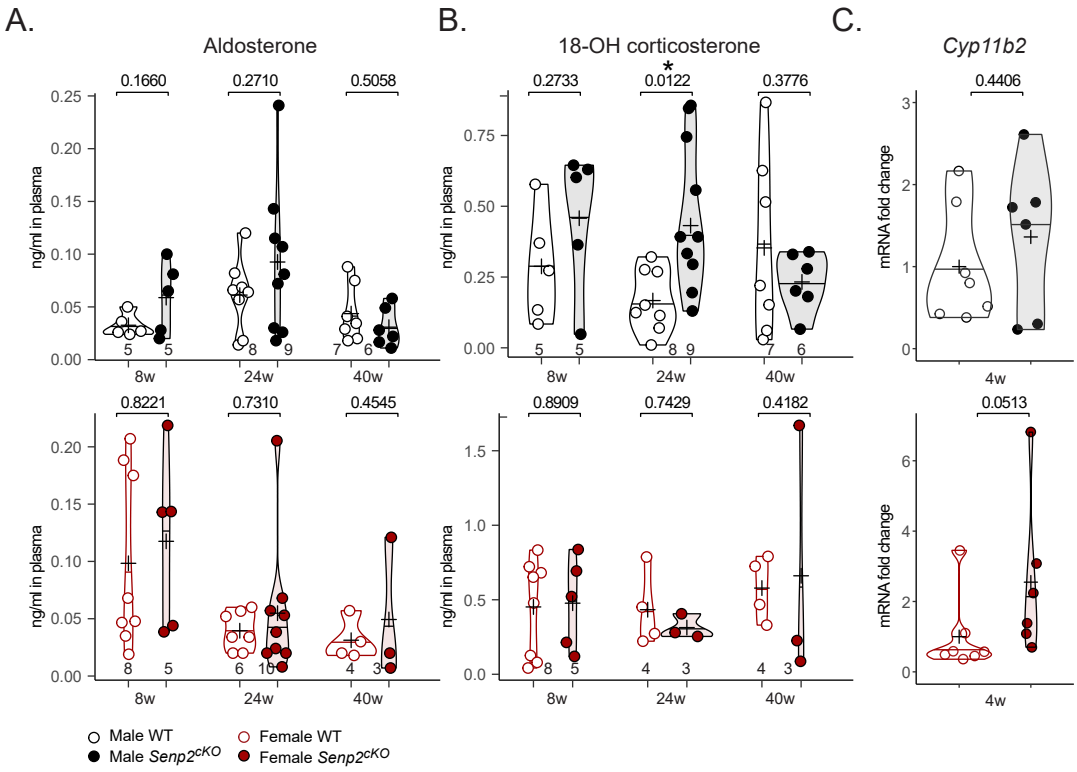

Fig.S 2: **Related to figure 2**
A. Plasmatic concentration of aldosterone in WT and $Senp2^{cKO}$ at 8, 24and 40 weeks of age (determined by LC-MS/MS).
B. Plasmatic concentration of 18-hydroxy-corticosterone in WT and $Senp2^{cKO}$ at 8, 24and 40 weeks of age (determined by LC-MS/MS).
C. qPCR analysis of aldosterone synthase coding gene *Cyp11b2* mRNA accumulation in 4-week-old WT and $Senp2^{cKO}$ adrenals.

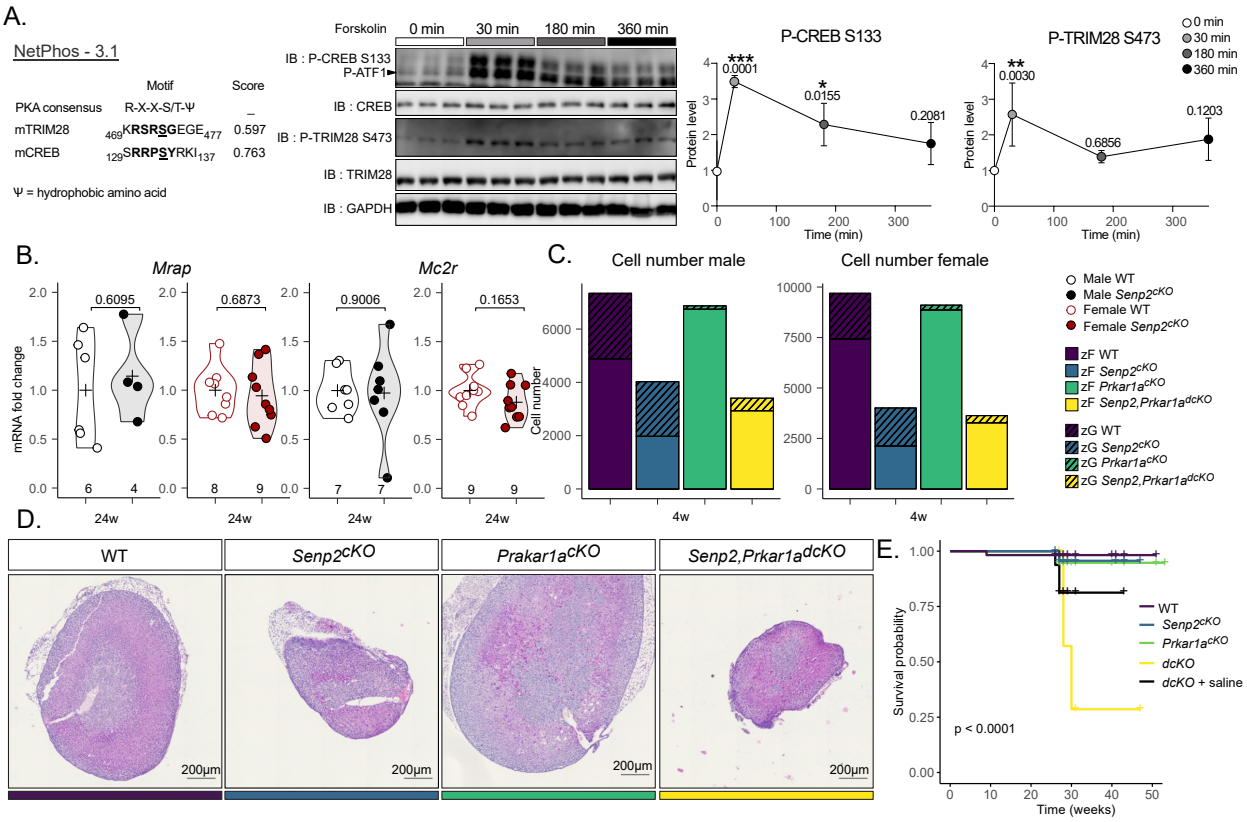

Fig.S 3: **Related to figure 3**

A. Left : PKA phosphorylation motifs on CREB and TRIM28 proteins as determined by NetPhos.3.1.
Right : Western blot analysis of the kinetics of CREB and TRIM28 phosphorylation after forskolin treatment in ATC7 cells. *P*-values represent difference between wells treated with vehicle compared to 30, 180 and 360 minutes of forskolin.
B. qPCR analysis of ACTH receptor and co-receptor mRNA accumulation in 24-week-old WT and $Senp2^{cKO}$ mice.
C. 2D cell counting number the adrenal cortex of male and female
D. Representative H&E staining of WT, $Senp2^{cKO}$, $Prkar1a^{cKO}$ or $Senp2,Prkar1a^{dcKO}$ adrenals
E. Kaplan-Meier curve of double-knockout mice with or without 0.9 % NaCl treatment

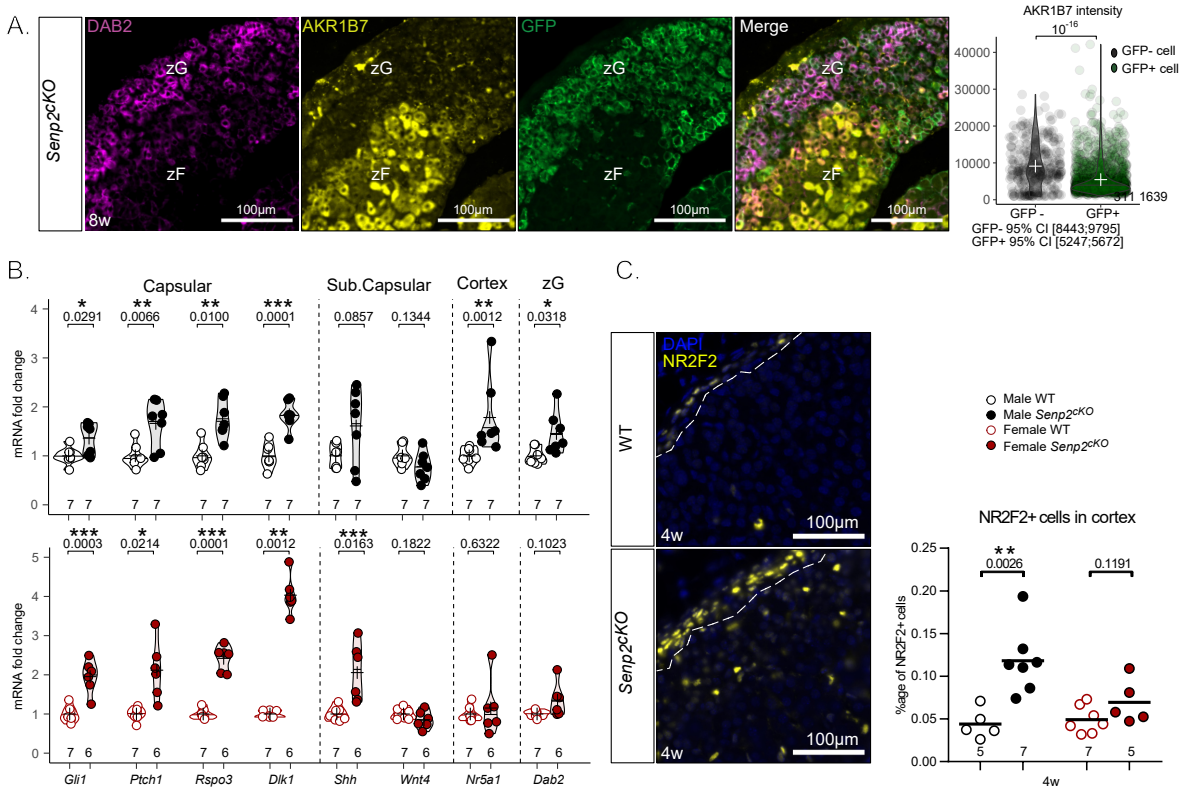

Fig.S 4: **Related to figure 4**

A. Coimmunofluorescent labelling of AKR1B7 (yellow), GFP (green) and Disabled2 (purple) on 8-week-old $Senp2^{cKO}$ female adrenal. Quantification of AKR1B7 intensity in GFP+ and GFP- $Senp2^{cKO}$ female adrenal cells

B. qPCR analysis of zonal marker mRNA accumulation in 4-week-old WT and $Senp2^{cKO}$ adrenals

C. Immunofluorescent labelling of capsular marker NR2F2 (yellow) with nuclei staining with DAPI (blue) and quantification of the proportion of NR2F2+ cells in the adrenal cortex of WT and $Senp2^{cKO}$ male and female adrenal cortices

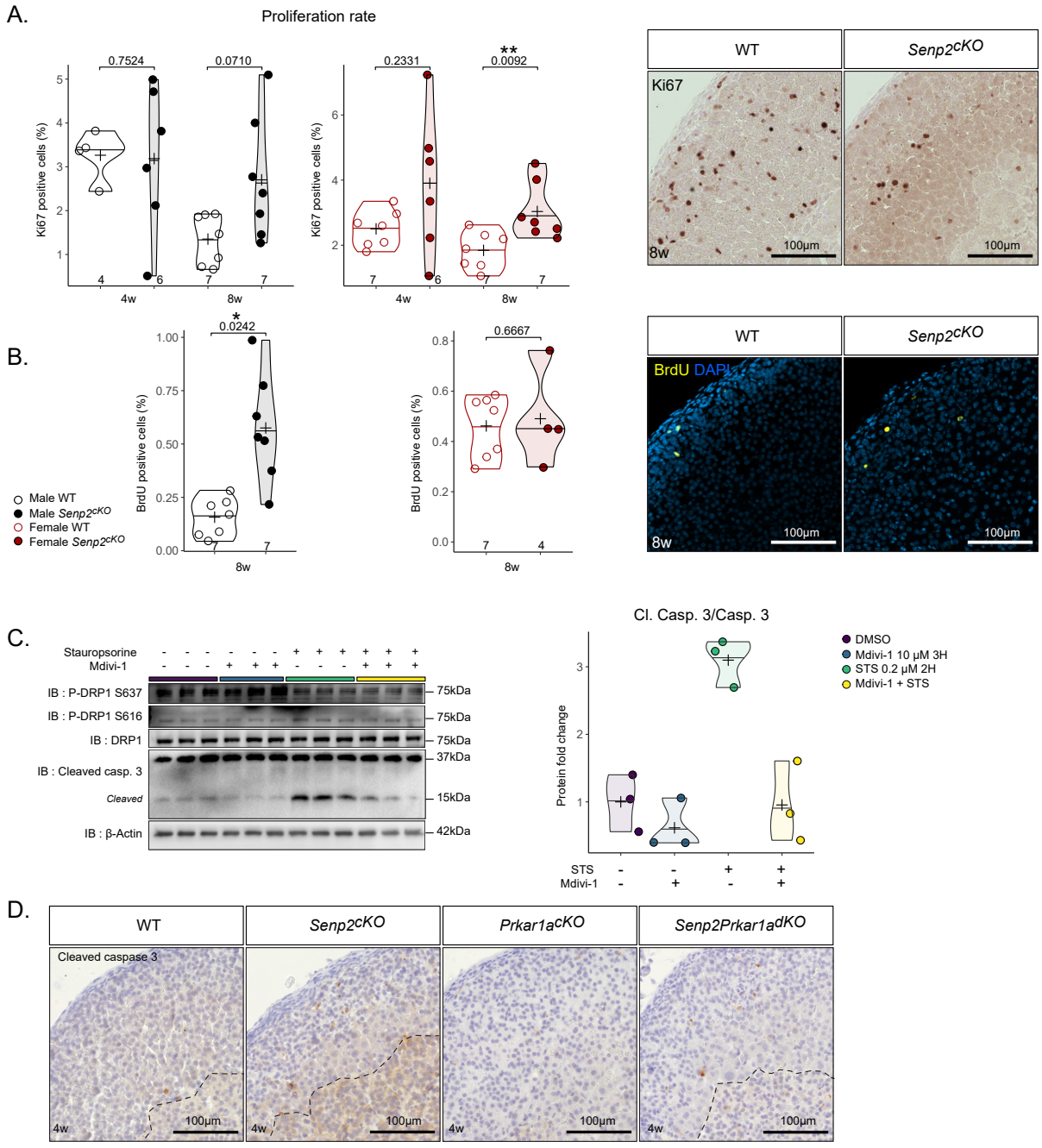

Fig.S 5: **Related to figure 5**

A. Quantification and representative picture of Ki67 staining on WT and *Senp2*^{cKO} 4- and 8-week-old adrenal cortices

B.Quantification and representative picture of 2 hours BrdU incorporation staining on WT and *Senp2*^{cKO} 8-week-old adrenal cortices

C. Western blot analysis of phosphorylated and total DRP1 in cells treated with DMSO, DRP1 inhibitor M-divi1 (10 µM) and/or Staurosporine (0.2 µM).

D. Immunostaining of cleaved caspase3 staining of WT, *Senp2*^{cKO}, *Prkar1a*^{cKO} or *Senp2,Prkar1a*^{dcKO} adrenals

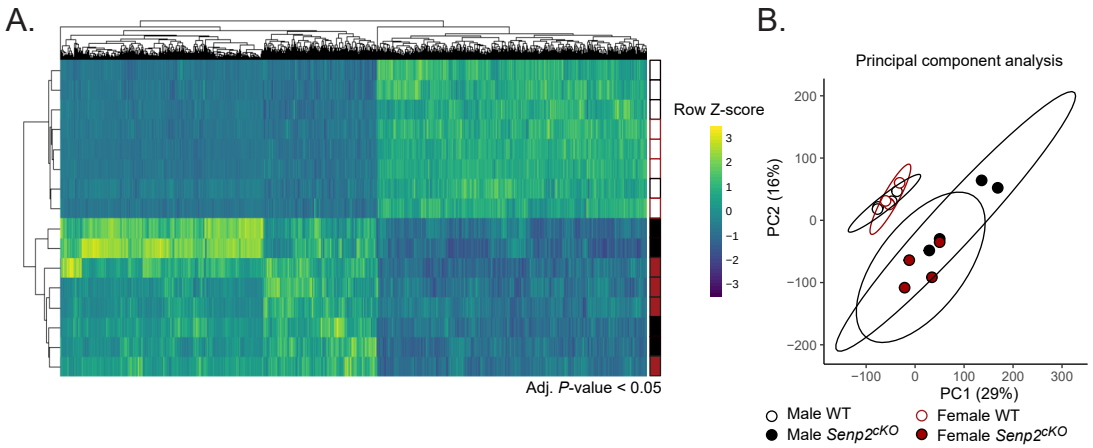

Fig.S 6: **Related to figure 6**
A. Heatmap representing the median centred expression of dysregulated genes (adjusted P-value < 0.05 between WT and $Senp2^{cKO}$ male or female) in 4-week-old male and female, WT and $Senp2^{cKO}$ adrenals
B. Principal component analysis of gene expression in WT and $Senp2^{cKO}$ 4-week-old male and female adrenals

References

1. King, P., Paul, A. & Laufer, E. Shh signaling regulates adrenocortical development and identifies progenitors of steroidogenic lineages. *Proceedings of the National Academy of Sciences* **106**, 21185–21190 (2009).

2. Freedman, B. D. *et al.* Adrenocortical Zonation Results from Lineage Conversion of Differentiated Zona Glomerulosa Cells. *Developmental Cell* **26**, 666–673 (2013).

3. Pignatti, E. *et al.* Beta-Catenin Causes Adrenal Hyperplasia by Blocking Zonal Transdifferentiation. *Cell Reports* **31**, 107524 (2020).

4. Berthon, A. *et al.* Constitutive beta-catenin activation induces adrenal hyperplasia and promotes adrenal cancer development. *Human Molecular Genetics* **19**, 1561–1576 (2010).

5. Berthon, A. *et al.* WNT/beta-catenin signalling is activated in aldosterone-producing adenomas and controls aldosterone production. *Human Molecular Genetics* **23**, 889–905 (2014).

6. Walczak, E. M. *et al.* Wnt Signaling Inhibits Adrenal Steroidogenesis by Cell-Autonomous and NonCell-Autonomous Mechanisms. *Molecular Endocrinology* **28**, 1471–1486 (2014).

7. Dumontet, T. *et al.* PKA signaling drives reticularis differentiation and sexually dimorphic adrenal cortex renewal. *JCI Insight* **3**, (2018).

8. Novoselova, T. V. *et al.* ACTH signalling and adrenal development: Lessons from mouse models. *Endocrine Connections* **8**, R122–R130 (2019).

9. Drelon, C. *et al.* PKA inhibits WNT signalling in adrenal cortex zonation and prevents malignant tumour development. *Nature Communications* **7**, 12751 (2016).

10. Mathieu, M. *et al.* Steroidogenic differentiation and PKA signaling are programmed by histone methyltransferase EZH2 in the adrenal cortex. *Proc Natl Acad Sci USA* **115**, E12265–E12274 (2018).

11. Minguez, P. *et al.* Deciphering a global network of functionally associated post-translational modifications. *Mol Syst Biol* **8**, 599 (2012).

12. *SUMO Regulation of Cellular Processes*. vol. 963 (Springer International Publishing, 2017).

13. Chang, H.-M. & Yeh, E. T. H. SUMO: From Bench to Bedside. *Physiological Reviews* **100**, 1599–1619 (2020).

14. Talamillo, A. *et al.* The role of SUMOylation during development. *Biochemical Society Transactions* **48**, 463–478 (2020).

15. Chung, S. S. *et al.* Control of Adipogenesis by the SUMO-Specific Protease SENP2. *Molecular and Cellular Biology* **30**, 2135–2146 (2010).

16. Cossec, J.-C. *et al.* SUMO Safeguards Somatic and Pluripotent Cell Identities by Enforcing Distinct Chromatin States. *Cell Stem Cell* **23**, 742–757.e8 (2018).

17. Liang, Q. *et al.* SENP2 Suppresses Necdin Expression to Promote Brown Adipocyte Differentiation. *Cell Reports* **28**, 2004–2011.e4 (2019).

18. Demarque, M. D. *et al.* Sumoylation by Ubc9 Regulates the Stem Cell Compartment and Structure and Function of the Intestinal Epithelium in Mice. *Gastroenterology* **140**, 286–296 (2011).

19. Ding, X. *et al.* Protein SUMOylation Is Required for Regulatory T Cell Expansion and Function. *Cell Reports* **16**, 1055–1066 (2016).

20. Dumontet, T. *et al.* Hormonal and spatial control of SUMOylation in the human and mouse adrenal cortex. *FASEB j.* **33**, 10218–10230 (2019).

21. Lee, F. Y. *et al.* Eliminating SF-1 (NR5A1) Sumoylation In Vivo Results in Ectopic Hedgehog Signaling and Disruption of Endocrine Development. *Developmental Cell* **21**, 315–327 (2011).

22. Qi, Y. *et al.* Hyper-SUMOylation of the Kv7 Potassium Channel Diminishes the M-Current Leading to Seizures and Sudden Death. *Neuron* **83**, 1159–1171 (2014).

23. Bingham, N. C., Verma-Kurvari, S., Parada, L. F. & Parker, K. L. Development of a steroidogenic factor 1/Cre transgenic mouse line. *genesis* **44**, 419–424 (2006).

24. Muzumdar, M. D., Tasic, B., Miyamichi, K., Li, L. & Luo, L. A global double-fluorescent Cre reporter mouse. *genesis* **45**, 593–605 (2007).

25. Levasseur, A., Dumontet, T. & Martinez, A. Sexual dimorphism in adrenal gland development and tumorigenesis. *Current Opinion in Endocrine and Metabolic Research* **8**, 60–65 (2019).

26. Lyraki, R. & Schedl, A. The Sexually Dimorphic Adrenal Cortex: Implications for Adrenal Disease. *IJMS* **22**, 4889 (2021).

27. Sahut-Barnola, I. *et al.* Cushing's Syndrome and Fetal Features Resurgence in Adrenal Cortex-Specific Prkar1a Knockout Mice. *PLoS Genetics* **6**, e1000980 (2010).

28. Kunz, K., Muller, S. & Mendler, L. Assays of SUMO protease/isopeptidase activity and function in mammalian cells and tissues. in *Methods in Enzymology* vol. 618 389–410 (Elsevier, 2019).

29. Grabek, A. *et al.* The Adult Adrenal Cortex Undergoes Rapid Tissue Renewal in a Sex-Specific Manner. *Cell Stem Cell* **25**, 290–296.e2 (2019).

30. Vinson, G. P. Functional Zonation of the Adult Mammalian Adrenal Cortex. *Front. Neurosci.* **10**, (2016).

31. Frank, S. *et al.* The Role of Dynamin-Related Protein 1, a Mediator of Mitochondrial Fission, in Apoptosis. *Developmental Cell* **1**, 515–525 (2001).

32. Sabouny, R. & Shutt, T. E. Reciprocal Regulation of Mitochondrial Fission and Fusion. *Trends in Biochemical Sciences* **45**, 564–577 (2020).

33. Chang, C.-R. & Blackstone, C. Cyclic AMP-dependent Protein Kinase Phosphorylation of Drp1 Regulates Its GTPase Activity and Mitochondrial Morphology. *J. Biol. Chem.* **282**, 21583–21587 (2007).

34. Park, J.-E. *et al.* Drp1 Phosphorylation Is Indispensable for Steroidogenesis in Leydig Cells. *Endocrinology* **160**, 729–743 (2019).

35. Plewes, M. R. *et al.* Luteinizing hormone regulates the phosphorylation and localization of the mitochondrial effector dynamin-related Protein1 (DRP1) and steroidogenesis in the bovine corpus luteum. *FASEB j.* fj.201902958R (2020) doi:10.1096/fj.201902958R.

36. Ragazzon, B. *et al.* Adrenocorticotropin-Dependent Changes in SF-1/DAX-1 Ratio Influence Steroidogenic Genes Expression in a Novel Model of Glucocorticoid-Producing Adrenocortical Cell Lines Derived from Targeted Tumorigenesis. *Endocrinology* **147**, 1805–1818 (2006).

37. Manczak, M., Kandimalla, R., Yin, X. & Reddy, P. H. Mitochondrial division inhibitor 1 reduces dynamin-related protein 1 and mitochondrial fission activity. *Human Molecular Genetics* **28**, 177–199 (2019).

38. Berthon, A., Martinez, A., Bertherat, J. & Val, P. Wnt/beta-catenin signalling in adrenal physiology and tumour development. *Molecular and Cellular Endocrinology* **351**, 87–95 (2012).

39. Kim, A. C. *et al.* Targeted disruption of beta-catenin in Sf1-expressing cells impairs development and maintenance of the adrenal cortex. *Development* **135**, 2593–2602 (2008).

40. Little, D. W., Dumontet, T., LaPensee, C. R. & Hammer, G. D. Beta-catenin in adrenal zonation and disease. *Molecular and Cellular Endocrinology* **522**, 111120 (2021).

41. Kadoya, T. *et al.* Desumoylation Activity of Axam, a Novel Axin-Binding Protein, Is Involved in Downregulation of beta-Catenin. *Mol Cell Biol* **22**, 3803–3819 (2002).

42. Kadoya, T. *et al.* Inhibition of Wnt Signaling Pathway by a Novel Axin-binding Protein. *Journal of Biological Chemistry* **275**, 37030–37037 (2000).

43. Nishida, T., Kaneko, F., Kitagawa, M. & Yasuda, H. Characterization of a Novel Mammalian SUMO-1/Smt3-specific Isopeptidase, a Homologue of Rat Axam, Which Is an Axin-binding Protein Promoting beta-Catenin Degradation. *J. Biol. Chem.* **276**, 39060–39066 (2001).

44. Huang, H.-J. *et al.* Beta-catenin SUMOylation is involved in the dysregulated proliferation of myeloma cells. *Am J Cancer Res* **5**, 309–320 (2015).

45. Karami, S. *et al.* Novel SUMO-Protease SENP7S Regulates beta-catenin Signaling and Mammary Epithelial Cell Transformation. *Scientific Reports* **7**, 46477 (2017).

46. Enserink, J. M. Sumo and the cellular stress response. *Cell Div* **10**, 4 (2015).

47. Buaas, F. W., Gardiner, J. R., Clayton, S., Val, P. & Swain, A. In vivo evidence for the crucial role of SF1 in steroid-producing cells of the testis, ovary and adrenal gland. *Development* **139**, 4561–4570 (2012).

48. Mosleh, E. *et al.* Ins1-Cre and Ins1-CreER Gene Replacement Alleles Are Susceptible To Silencing By DNA Hypermethylation. *Endocrinology* **161**, bqaa054 (2020).

49. Lopez, J. P. *et al.* Single-cell molecular profiling of all three components of the HPA axis reveals adrenal ABCB1 as a regulator of stress adaptation. *Sci. Adv.* **7**, eabe4497 (2021).

50. Chida, D. *et al.* Melanocortin 2 receptor is required for adrenal gland development, steroidogenesis, and neonatal gluconeogenesis. *Proceedings of the National Academy of Sciences* **104**, 18205–18210 (2007).

51. Novoselova, T. V. *et al.* MRAP deficiency impairs adrenal progenitor cell differentiation and gland zonation. *FASEB j.* **32**, 6186–6196 (2018).

52. Choi, H.-K. *et al.* Reversible SUMOylation of TBL1-TBLR1 Regulates beta-Catenin-Mediated Wnt Signaling. *Molecular Cell* **43**, 203–216 (2011).

53. Cai, Z. *et al.* Redox-sensitive enzyme SENP3 mediates vascular remodeling via de-SUMOylation of beta-catenin and regulation of its stability. *EBioMedicine* **67**, 103386 (2021).

54. Leng, S. *et al.* Beta-Catenin and FGFR2 regulate postnatal rosette-based adrenocortical morphogenesis. *Nat Commun* **11**, 1680 (2020).

55. Rossitto, M. *et al. TRIM28-dependent SUMOylation protects the adult ovary from the male pathway.* http://biorxiv.org/lookup/doi/10.1101/2021.03.24.436749 (2021) doi:10.1101/2021.03.24.436749.

56. Tan, S. *et al.* Stromal Senp1 promotes mouse early folliculogenesis by regulating BMP4 expression. *Cell Biosci* **7**, 36 (2017).

57. Lee, J. S. *et al. SUMO-specific protease 2 (SENP2) suppresses browning of white adipose tissue through C/EBPbeta modulation.* http://biorxiv.org/lookup/doi/10.1101/2020.12.16.422969 (2020) doi:10.1101/2020.12.16.422969.

58. Lopez, I. *et al.* An unanticipated tumor-suppressive role of the SUMO pathway in the intestine unveiled by Ubc9 haploinsufficiency. *Oncogene* **39**, 6692–6703 (2020).

59. Yin, M. *et al.* CD34+KLF4+ Stromal Stem Cells Contribute to Endometrial Regeneration and Repair. *Cell Reports* **27**, 2709–2724.e3 (2019).

60. Jang, S. M. *et al.* KAP1 facilitates reinstatement of heterochromatin after DNA replication. *Nucleic Acids Research* **46**, 8788–8802 (2018).

61. Li, M., Xu, X., Chang, C.-W. & Liu, Y. TRIM28 functions as the SUMO E3 ligase for PCNA in prevention of transcription induced DNA breaks. *Proc Natl Acad Sci USA* **117**, 23588–23596 (2020).

62. Leclerc, J., Ballotti, R. & Bertolotto, C. Pathways from senescence to melanoma: Focus on MITF sumoylation. *Oncogene* **36**, 6659–6667 (2017).

63. Batisse-Lignier, M. *et al.* P53/Rb inhibition induces metastatic adrenocortical carcinomas in a preclinical transgenic model. *Oncogene* **36**, 4445–4456 (2017).

64. Travers, S. *et al.* Multiplexed steroid profiling of gluco- and mineralocorticoids pathways using a liquid chromatography tandem mass spectrometry method. *The Journal of Steroid Biochemistry and Molecular Biology* **165**, 202–211 (2017).

65. Bankhead, P. *et al.* QuPath: Open source software for digital pathology image analysis. *Sci Rep* **7**, 16878 (2017).

66. Subramanian, A. *et al.* Gene set enrichment analysis: A knowledge-based approach for interpreting genome-wide expression profiles. *Proceedings of the National Academy of Sciences* **102**, 15545–15550 (2005).

67. Raudvere, U. *et al.* G:Profiler: A web server for functional enrichment analysis and conversions of gene lists (2019 update). *Nucleic Acids Research* **47**, W191–W198 (2019).

68. R Core Team. *R: A language and environment for statistical computing*. (R Foundation for Statistical Computing, 2018).

IHC

Antibody	Manufacturer	Reference	host	unmasking	Saturation	dilution
AKR1B7	Santa Cruz	SC-27763	goat	CT	Horse serum 2.5%	1/200
TH	Antibodies online	AA 30 100	goat	CT	Horse serum 2.5%	1/1000
TH	Chemicon	AB 152	rabbit	CT	Horse serum 2.5%	1/500
DAB2	BD bioscience	610464	mouse	CT	Horse serum 2.5%	1/500
Laminin	Sigma Aldrich	L9393	rabbit	TE	Horse serum 2.5%	1/200
GFP	invitrogen	A11122	rabbit	CT	Horse serum 2.5%	1/1500
GFP	Abcam	Ab5450	goat	CT/TE	Horse serum 2.5%	1/1000
Tomato/RFP	Rockland	600-401-379	rabbit	TE	Horse serum 2.5%	1/1000
SF1	Cosmo Bio	KAL-KO610	rat	TE	Horse serum 2.5%	1/100
CYP21	Sigma Aldrich	HPA 048979	rabbit	CT	Horse serum 2.5%	1/500
Cleaved Caspase3	Cell signaling	CST9661	rabbit	CT	Horse serum 2.5%	1/200
Active β-catenin	Cell signaling	CST4270	rabbit	CT	Horse serum 2.5%	1/500
β-catenin	BD bioscience	397555	mouse	CT	Horse serum 2.5%	1/500
SUMO2/3		8A2	mouse	CT	Horse serum 2.5%	1/200
NR2F2	Perseus	PPDH7147D00!	mouse	V	Horse serum 2.5%	1/200
Ki67	Abcam	Ab15580	rabbit	CT	Horse serum 2.5%	1/3000
BrdU	Roche	11170376001	mouse	CT	Horse serum 2.5%	1/400
GATA6	Cell signaling	CST5851	rabbit	CT	Horse serum 2.5%	1/1600
SUMO2/3	Abcam	Ab3742	rabbit	CT	Horse serum 2.5%	1/200

Western Blot

Antibody	Manufacturer	Reference	host	Saturation	dilution
P-CREB S133	Cell signaling	CST9198	rabbit	BSA 5%	1/500
CREB	Cell signaling	CST9197	rabbit	BSA 5%	1/1000
β-actin	Sigma-Aldrich	2066	rabbit	BSA 5%	1/10000
P-DRP1 S637	Cell signaling	CST4867	rabbit	BSA 5%	1/200
P-DRP1 S616	Cell signaling	CST3455	rabbit	BSA 5%	1/200
DRP1	NOVUS	NB55237	rabbit	BSA 5%	1/500
Cleaved Caspase3	Cell signaling	CST9661	rabbit	BSA 5%	1/500
β-catenin	BD bioscience	397555	mouse	BSA 5%	1/1000
SUMO2/3		8A2	mouse	BSA 5%	1/200
SUMO2/3	Abcam	Ab3742	rabbit	BSA 5%	1/500
GAPDH	NOVUS	NB30021	rabbit	BSA 5%	1/10000
SUMO1	Cell signaling	CST4930	rabbit	BSA 5%	1/500
TRIM28	Bethyl	BETA700-014-T	rabbit	BSA 5%	1/1000
P-TRIM28 S473	Biolegend	BLE654101	mouse	BSA 5%	1/1000
PKA Cαβ	BD bioscience	610981	mouse	BSA 5%	1/500
HA	Abcam	ab9110	rabbit	BSA 5%	1/5000

Gene name	FW	RV
Akr1b7	GCCAGTGACCAACCAGATTGAGA	ACGGGGTCTTCTGGCTTGGCAT
Apcdd1	CTCAGCCCCACACTCATTCC	TGGCACGGAGTTTGTGTTCA
Axin2	TGGGGAGTAAGAAACAGCTCC	AGCCTTTGACCAGCACTGAG
Ccdc80	AGGCATGCAATTTTGGTCTGC	ACATCTTCCCGCTCAACGAT
Cyp11a1	CTGCCTCCAGACTTCTTTCG	TTCTTGAAGGGCAGCTTGTT
Cyp11b1	GCAGAGATGATGCTCCTGCTT	GAGAGGGCAATGTGTCATCAGAA
Cyp11b2	ATGCTGAGAAGTTGCACCAG	ATTCTGGCCCATTTAGCAAG
Cyp21a1	GCTGTGGCTTTCCTGCTTCAC	GGCCCAGCTTGAGGTCTAACT
Dab2	CCTGCATCTTCTGATCCCCAC	CATGTTTCTGGCTGTCTGCTT
Dlk1	CTCCTGCGCGTCCTCTTGCTC	CTGCAGACATTGTCAGCCTCGCAG
Gli1	CCTGGTGGCTTTCATCAACTCTCG	CACAGGGCTGGACTCCATAGG
Hsd3b1	ATGGTCTGCCTGGGAATGAC	ACTGCAGGAGGTCAGAGCT
Lef1	GACGAGCACTTTTCTCCGGG	TGGGGTGATCTGTCCAACGC
Mc2r	CAAACACCACCCCCGTCTTA	TCTTGCGGTGTCATTGGTGT
Mrap	CAGAAGCCCTACAGGGGAAC	AGAATCACCCGGCTTGTCTG
Nr5a1	TGCAGAATGGCCGACCAG	TGGCGGTAGATGTGGTC
Ptch1	CCATACACCAGCCACAGCTTCG	GGAGGCTGGAGTCTGAGAACTG
Rspo3	TCATTTTGAACTTTATGGAATACATTG	CAGCCATTGTAATCTGAACACG
Scarb1	CCTTCGTGGAGAACCGCAGCC	CCCATGGTGACCAGCGCCAA
Senp2	GCGGAGACATCCAGACCTTA	AGGCTCCAATGTACCTTCCG
Shh	GCGGCAGATATGAAGGGAAGATC	GTTCATCACAGAGATGGCCAAGGC
Star	TCGCTACGTTCAAGCTGTGT	ACGTCGAACTTGACCCATCC
Wnt4	CCCTGTCTTTGGGAAGGTGGTG	CACCTGCTGAAGAGATGGCGTATAC
36b4	GTCACTGTGCCAGCTCAGAA	CAATGGTGCCTCTGGAGAT
Senp2 (genomic DNA)	ACTTCACAACAGTGAGGACT	AAGTGCAGGAGGAGGTGGATTCAA
Senp2 (genomic DNA)	CTTCTGCTTCTCTTAGTGCT	AAGAGCAAGCACTCTTACTG